



**University of
Zurich^{UZH}**

**Zurich Open Repository and
Archive**

University of Zurich
University Library
Strickhofstrasse 39
CH-8057 Zurich
www.zora.uzh.ch

Year: 2019

Cryptic chlorophyll breakdown in non-senescent green *Arabidopsis thaliana* leaves

Süssenbacher, Iris ; Menghini, Damian ; Scherzer, Gerhard ; Salinger, Kathrin ; Erhart, Theresia ; Moser, Simone ; Vergeiner, Clemens ; Hörtensteiner, Stefan ; Kräutler, Bernhard

Abstract: Chlorophyll (Chl) breakdown is a diagnostic visual process of leaf senescence, which furnishes phyllobilins (PBs) by the PAO/phyllobilin pathway. As Chl breakdown disables photosynthesis, it appears to have no role in photoactive green leaves. Here, colorless PBs were detected in green, non-senescent leaves of *Arabidopsis thaliana*. The PBs from the green leaves had structures entirely consistent with the PAO/phyllobilin pathway and the mutation of a single Chl catabolic enzyme completely abolished PBs with the particular modification. Hence, the PAO/phyllobilin pathway was active in the absence of visible senescence and expression of genes encoding Chl catabolic enzymes was observed in green *Arabidopsis* leaves. PBs accumulated to only sub-% amounts compared to the Chls present in the green leaves, excluding a substantial contribution of Chl breakdown from rapid Chl turnover associated with photosystem II repair. Indeed, Chl turnover was shown to involve a Chl a dephytylation and Chl a reconstitution cycle. However, non-recyclable pheophytin a is also liberated in the course of photosystem II repair, and is proposed here to be scavenged and degraded to the observed PBs. Hence, a cryptic form of the established pathway of Chl breakdown is indicated to play a constitutive role in photoactive leaves.

DOI: <https://doi.org/10.1007/s11120-019-00649-2>

Posted at the Zurich Open Repository and Archive, University of Zurich

ZORA URL: <https://doi.org/10.5167/uzh-183048>

Journal Article

Accepted Version

Originally published at:

Süssenbacher, Iris; Menghini, Damian; Scherzer, Gerhard; Salinger, Kathrin; Erhart, Theresia; Moser, Simone; Vergeiner, Clemens; Hörtensteiner, Stefan; Kräutler, Bernhard (2019). Cryptic chlorophyll breakdown in non-senescent green *Arabidopsis thaliana* leaves. *Photosynthesis Research*, 142(1):69-85.

DOI: <https://doi.org/10.1007/s11120-019-00649-2>

Cryptic Chlorophyll Breakdown in Non-Senescent Green

***Arabidopsis thaliana* Leaves**

Iris Süssenbacher^{1*}, Damian Menghini^{2*}, Gerhard Scherzer¹, Kathrin Salinger², Theresia Erhart¹, Simone Moser¹, Clemens Vergeiner¹, Stefan Hörtensteiner² and Bernhard Kräutler¹

¹Institute of Organic Chemistry and Centre of Molecular Biosciences, University of Innsbruck, Innrain 80/82, 6020 Innsbruck, Austria

²Institute of Plant and Microbial Biology, University of Zürich, Zollikerstrasse 107, 8008 Zürich, Switzerland

*equal contribution

Corresponding authors

Stefan Hörtensteiner (shorten@botinst.uzh.ch) and
Bernhard Kräutler (bernhard.kraeutler@uibk.ac.at)

ORCID numbers:

Stefan Hörtensteiner 0000-0002-3751-5089

Bernhard Kräutler 0000-0002-2222-0587

Acknowledgements

This work was supported by Austrian Science Fund (FWF, project P-28522 to B.K.) and the Swiss National Foundation (project 31003A_172977 to S.H.).

Abstract. Chlorophyll (Chl) breakdown is a diagnostic visual process of leaf senescence, which furnishes phyllobilins (PBs) by the PAO/phyllobilin pathway. As Chl breakdown disables photosynthesis, it appears to have no role in photoactive green leaves. Here, colorless PBs were detected in green, non-senescent leaves of *Arabidopsis thaliana*. The PBs from the green leaves had structures entirely consistent with the PAO/phyllobilin pathway and the mutation of a single Chl catabolic enzyme completely abolished PBs with the particular modification. Hence, the PAO/phyllobilin pathway was active in the absence of visible senescence and expression of genes encoding Chl catabolic enzymes was observed in green *Arabidopsis* leaves. PBs accumulated to only sub-% amounts compared to the Chls present in the green leaves, excluding a substantial contribution of Chl breakdown from rapid Chl turnover associated with photosystem II repair. Indeed, Chl turnover was shown to involve a Chl *a* dephytylation and Chl *a* reconstitution cycle. However, non-recyclable pheophytin *a* is also liberated in the course of photosystem II repair, and is proposed here to be scavenged and degraded to the observed PBs. Hence, a cryptic form of the established pathway of Chl breakdown is indicated to play a constitutive role in photoactive leaves.

Keywords

chlorophyll breakdown; chlorophyll turnover; PAO/phyllobilin pathway; pheophytin; phyllobilin; photosystem II repair

Introduction

Breakdown of chlorophyll (Chl) is a visual sign of leaf senescence and fruit ripening, associated with the appearance of the colors of fall leaves and ripe fruit (Hörtensteiner and Kräutler 2011). Various forms of stress, such as low light, drought, pathogen infections, as well as developmental processes, like flowering induction are among the known internal and external factors leading to leaf senescence (Christ et al. 2014; Kusaba et al. 2013; Lim et al. 2007; Mittelberger et al. 2017). In senescent leaves, Chl breakdown is an efficient means of Chl detoxification, enabling the simultaneous remobilization of nutrients from Chl-binding proteins, in particular nitrogen (Hörtensteiner 2009; Kräutler and Hörtensteiner 2014). However, the loss of Chl disables photosynthesis, thus, impairing essential metabolic activities in leaf cells during senescence. Therefore, net loss of Chl during the photosynthetic phase has to be prevented (Matile et al. 1999). Chl breakdown furnishes a variety of bilin-type catabolites (Fig. 1), named phyllobilins (PBs), whose potential physiological roles in plants

are still unclear (Kräutler 2014; Kräutler 2016). Chl has also been considered to be turned over and transformed in green leaves as demonstrated, indeed, by pulse-chase isotope-labeling of Chl in green leaves of several plant species (Beisel et al. 2010; Feierabend and Dehne 1996; Lin et al. 2016; Perkins and Roberts 1963) and at the stationary phase of growth in algal and cyanobacterial cultures (Grumbach et al. 1978; Riper et al. 1979; Vavilin and Vermaas 2007). In particular, photo-oxidative damage of photosystem II (PS II) is a consequence of light excitation during photosynthesis (Aro et al. 1993), requiring constant and rapid repair of the reaction center subunit D1 (Komenda et al. 2012; Theis and Schroda 2016). Turnover of D1-bound Chl has been proposed to accompany D1 protein recycling (Feierabend and Dehne 1996), although the biochemical mechanism of Chl turnover is largely unknown. ^{15}N and ^{14}C -isotope-labeling experiments in *Synechocystis* indicated the reutilization for Chl re-synthesis of substantial portions of chlorophyllide (Chlide) and phytol derived from Chl hydrolysis (Vavilin and Vermaas 2007). In *Arabidopsis thaliana* (Arabidopsis), CHLOROPHYLL DEPHYTYLASE 1 (CLD1) and CHLOROPHYLL SYNTHASE (CHLG), catalyzing Chl hydrolysis to Chlide and Chl re-synthesis, respectively, have been identified to be involved in a Chl salvage process during heat stress, i.e. conditions with high Chl turnover (Lin et al. 2014; Lin et al. 2016). These findings imply that during turnover, Chl may be salvaged for re-synthesis rather than degraded substantially, beyond the level of Chlide. The aim of our work was to investigate Chl breakdown in green leaves and to find a possible link of the PAO/phyllobilin pathway of Chl breakdown with the frequently inferred Chl turnover.

Chl breakdown in higher plants follows the largely common PAO/phyllobilin pathway, in which the red Chl catabolite (RCC) (Kräutler et al. 1997; Rodoni et al. 1997) and the colorless ‘primary’ fluorescent Chl catabolite (pFCC) (Mühlecker et al. 1997) are key ring-opened formylxobilin-type intermediates. pFCC is generated from green pheophorbide *a* (Pheide *a*) (Hörtensteiner et al. 1995) by the action of the monooxygenase PHEOPHORBIDE A OXYGENASE (PAO) (Pružinská et al. 2003) and RCC REDUCTASE (RCCR) (Wüthrich et al. 2000) (Fig. 1). In senescent leaves, the formation of Pheide *a* from Chl *a* involves two preceding activities, i.e. de-metalation catalyzed by STAY-GREEN 1 (SGR1) and SGR2 (Ren et al. 2007; Shimoda et al. 2016; Wu et al. 2016), and subsequent dephytylation of pheophytin *a* (Phein *a*) through PHEOPHYTIN PHEOPHORBIDE HYDROLASE (PPH) (Schelbert et al. 2009). Both SGR and PAO show a remarkable specificity for “*a*-type” pigments (Hörtensteiner et al. 1995; Shimoda et al. 2016), rationalizing the fact that before further breakdown, Chl *b* is converted to Chl *a* (Scheumann et al. 1999; Shimoda et al. 2012), and

that PBs relate to Chl *a* (Kräutler 2016). The reduction of Chl *b* to Chl *a* is a two-step reaction and is catalyzed by NON-YELLOW COLORING 1 (NYC1)/NYC1-LIKE (NOL) (Horie et al. 2009; Kusaba et al. 2007) and HYDROXYCHLOROPHYLL A REDUCTASE (HCAR) (Meguro et al. 2011), respectively. In senescent leaves of *Arabidopsis* and some other plants, *p*FCC is the precursor of downstream formylxobilin-type PBs, classified as type-I PBs, as well as of dioxobilin-type PBs (classified as type-II PBs) (Kräutler 2014; Kräutler 2016). In senescent *Arabidopsis* leaves the main PBs are type-II PBs, such as the dioxobilin-type FCC *At*-DFCC-33, and its natural nonfluorescent isomer, *At*-DNCC-33 (Fig. 1) (Christ et al. 2016; Christ et al. 2013; Süssenbacher et al. 2015a). In *Arabidopsis*, formation of type-II PBs results from the activity of the endoplasmic reticulum-localized CYTOCHROME P450 MONOOXYGENASE 89A9 (CYP89A9), which removes the C1-formyl group of FCCs (Christ et al. 2013). Two further modifications are involved in the formation of *At*-DFCC-33, i.e., hydroxylation of *p*FCC at the C3² position, catalyzed by the chloroplast-localized protein TRANSLOCON AT THE INNER CHLOROPLAST ENVELOPE 55 (TIC55) (Hauenstein et al. 2016), and hydrolysis of the methyl ester group at C8² of the hypothetical methyl ester precursor of *At*-DFCC-33, catalyzed by the cytosolic METHYLESTERASE 16 (MES16) (Christ et al. 2012). After import into the acidic vacuole, the blue fluorescent FCCs and DFCCs convert rapidly into their nonfluorescent isomers, the corresponding NCCs (Oberhuber et al. 2003; Oberhuber et al. 2008) or dioxobilin-type NCCs (DNCCs), respectively (Süssenbacher et al. 2015a).

Using defined, non-senescent leaves of *Arabidopsis* wild type and of mutants that were defective in the FCC-modifying Chl catabolic enzymes (CCEs) TIC55, CYP89A9 and/or MES16, colorless PBs were, strikingly, found in green, pre-senescent leaves, as reported herein. Our data indicate Chl degradation by the PAO/phyllobilin pathway in green leaves. However, in such pre-senescent leaves PBs occur only in low abundancies, implying that breakdown of Chl to PBs in green leaves is a minor process, compared to the overall turnover of Chl considered to take place at this pre-senescent leaf stage.

Materials and methods

Plant material and growth

In this study, *Arabidopsis thaliana* (*Arabidopsis*) ecotype Columbia-0 (Col-0) was used as the wild type. The T-DNA insertion lines of the three CCEs methylesterase 16 (MES16), i.e. *mes16-1*, cytochrome P450 89A9 (CYP89A9), i.e. *cyp89a9-1*, and translocon at the inner

chloroplast envelope 55 (TIC55), i.e. *tic55-3*, have been described elsewhere (Christ et al. 2012; Christ et al. 2013; Hauenstein et al. 2016). In addition, a *cyp89a9-1/mes16-1* double mutant (Christ et al. 2016) was analyzed.

Plants were grown on soil in a controlled growth chamber under fluorescent light of 100-120 $\mu\text{mol photons m}^{-2}\text{s}^{-1}$ in an 8 h light/16 h dark regime (short day) at 22°C with constant relative humidity of 60%. For the experiments, leaf #6 and #8 of 6-week-old plants (42 days after sowing, DAS) were used. To help identifying these leaves, u-shaped metal wires were placed over the petioles of respective leaves at 28 DAS (Fig. 2A). At 42 DAS, individual leaves ($n = 6$) were harvested at the end of the 8 h light period (providing samples d0-l). Further sets of leaves were collected after the subsequent 16 h dark period, i.e. before switch on of the light at 43 DAS (samples d1-d), after an 8 h light period at 49 DAS (samples d7-l) and after the subsequent 16 h dark period at 50 DAS (samples d8-d), furnishing for each genotype a total of 24 samples each for leaf #6 and leaf #8 (Fig. 2A) for analysis of chlorophyll catabolites. In addition, at each time point two replicates of Col-0 leaf #8 were collected for gene expression analysis. Sampling at the end of the dark period was done under green safe light. Leaves were collected in 2-mL Eppendorf tubes containing 300-500 μL of glass beads (1.25-1.65 mm diameter), weighed and quickly frozen with liquid nitrogen. The frozen samples were homogenized using a mixer mill (MM300, Retsch) and stored at -80°C until Chl determination, gene expression analyses, and PB analyses by HPLC and by LC/ESI-MS (see below).

Naturally senescent leaves

Wild type Arabidopsis plants were grown for two weeks with 8 h light/16 h dark periods before being transferred to a 16 h light/8 h dark regime for another four to five weeks. Five leaves that had mostly become bright yellow were harvested and frozen with liquid N_2 . The frozen leaf samples were suspended cold in 50 μL MeOH and the cold leaf suspension was crushed in a mortar. The leaf slurry was transferred into an Eppendorf tube, which was warmed up to RT and centrifuged for 10 min at 13000 rpm. The supernatants were removed and mixed 1:1 (v/v) with MeOH/50 mM K-phosphate buffer pH 7 (1:4; v/v) and centrifuged again for 3 min. The supernatant was removed and used for the analyses by HPLC (with UV detection, solvent system A) and by LC/ESI-MS (see below).

Chemicals

HPLC grade methanol (MeOH) was from VWR (West Chester, USA), ultra-pure water

($18\text{M}\Omega\text{ cm}^{-1}$) from a Millipore apparatus. Potassium phosphate monobasic (KH_2PO_4), puriss. p.a., potassium phosphate dibasic (K_2HPO_4), puriss. p.a. were from Fluka (Buchs, Switzerland). Chlorophyll catabolites: NCC-1 was isolated from senescent leaves of *Cercidiphyllum japonicum* (named *Cj*-NCC-1 earlier) (Curty and Engel 1996; Oberhuber et al. 2003), Vv-DNCC-51 from senescent grapevine leaves (Erhart et al. 2018), *At*-NCC-5 (Pružinská et al. 2005) and *At*-4HM-DNCC-41 (Süssenbacher et al. 2015b) were from wild type *A. thaliana*.

Chromatography

Analytical HPLC. Stationary phase & columns: Phenomenex Hyperclone ODS 5 μm 250x4.6 mm i.d. column, with Phenomenex ODS 4x3 mm i.d. pre-column; mobile phase A = 50 mM potassium phosphate buffer pH 7, B = MeOH, flow 0.5 mL/min; solvent composition A: 0-5 min 20% B, 5 to 55 min 20% B to 70% B, 55 to 60 min 70% B to 100%; absorbance detection at 250 nm and at 320 nm, fluorescence detection at 450 nm (with excitation at 350 nm). B. **HPLC System I** (used for leaf samples #6): Agilent HPLC system with a 1260 Infinity Degasser, a 1100 Series quaternary pump, detection of absorbance at 254 nm and 320 nm with a 1100 Series diode array and fluorescence at 450 nm with a FLD-G1321A fluorescence detector. Rheodyne injection valve with 200 μL loop; Data were processed with HP ChemStations. **HPLC System II** (used for leaf samples #8): Dionex Summit HPLC system with manual sampler and online degasser, P680 HPLC pump, detection of absorbance at 250 nm and 320 nm by UVD340U diode array and fluorescence at 450 nm with Dionex RF 2000 fluorescence detector and a Rheodyne injection valve with 200 μL loop; Data were processed with Chromeleon 6.50.

Calibration of HPLC Systems. For calibration of HPLC system I, a 61 μM stock solution of *At*-NCC-5 (Pružinská et al. 2005) (for detailed spectroscopic data of *At*-NCC-5, see below and Supplementary Figs. 5–7) in H_2O was used, which was diluted by the factors 2, 8, 32, and 128. HPLC peak areas at $\lambda = 320\text{ nm}$ of the resulting solutions were used to produce a linear regression. Corresponding peak areas at 254 nm for each catabolite type were calculated from this linear regression, using the following correction factors: for NCCs: $\epsilon_{254}(\text{At-NCC-5})/\epsilon_{320}(\text{At-NCC-5}) = 1.05$ (Supplementary Fig. 8), for an FCC: $\epsilon_{254}(\text{FCC})/\epsilon_{320}(\text{At-NCC-5}) = 1.01$ (Vergeiner et al. 2013) and for DNCCs: $\epsilon_{254}(\text{DNCC})/\epsilon_{320}(\text{At-NCC-5}) = 1.17$ (Supplementary Fig. 8). HPLC system II was calibrated using a 31 μM stock solution of NCC-1 in 50 mM aqueous potassium phosphate buffer pH 7/MeOH (1:4; v/v), which was diluted 10, 20 and 40 times. HPLC peak areas at $\lambda = 320\text{ nm}$ of the resulting solutions were

used to produce a linear regression. Based on this linear regression, and by applying the correction factor $\epsilon_{320}(\text{FCC})/\epsilon_{320}(\text{NCC-1}) = 1.19$ (Vergeiner et al. 2013), the corresponding peak areas at 320 nm were used for quantification of NCCs and FCCs, respectively. For DNCCs, the calibration was carried out analogously with a 32 μM stock solution of Vv-DNCC-51 (Erhart et al. 2018), and using peak areas at $\lambda = 250$ nm for calculating the linear regression (Supplementary Fig. 8).

LC/ESI-MS. Ultimate Nano-HPLC system, Dionex UVD 340S diode array detector, Phenomenex Hyperclone ODS (5 μm 250x4.6 mm i.d. column, with Phenomenex ODS 4x3 mm i.d. pre-column and a Rheodyne injection valve with 30 μL loop; mobile phase A = 4 mM aqueous ammonium acetate buffer pH 7, B = MeOH, flow 0.5 mL/min; solvent composition: 0-5 min 20% B, 5 to 55 min 20% B to 70% B, 55 to 60 min 70% B to 100%; absorbance detection at 250 nm and at 320 nm; coupled with Finnigan LCQclassic, 4.5 kV spray voltage, positive ion detection.

Production of leaf extracts for analysis of phyllobilins

From each leaf batch three frozen samples were first extracted cold with 70 μL of a solvent mixture of 50 mM potassium phosphate buffer pH 7)/MeOH (4:1; v/v). The supernatant was removed after centrifugation at 13 000 rpm (5 min), the solid residue re-suspended in 100 μL of the solvent mixture, centrifuged and the supernatant was removed again. The two supernatants were pooled and centrifuged. The resulting clear supernatants were directly injected for reversed phase HPLC analysis. PBs of a particular set of Arabidopsis leaves of each of the mutants were present in small and rather reproducible amounts, differing from one set to the other, depending upon sampling time and leaf number. All of the major PBs found here, were identified with known PBs from leaves of corresponding Arabidopsis mutants, using a combination of HPLC analysis with UV detection, complemented by LC/ESI-MS analysis of a complete set of extracts of leaves #6. The PBs were characterized by their UV-spectral and mass spectrometric data as FCCs, NCCs or DNCCs, and named here by inclusion of their HPLC analytical retention time, as provided by HPLC system I.

RNA extraction and gene expression analysis by quantitative real-time PCR

RNA was extracted from homogenized leaf samples using the RNeasy Plant Mini kit (Qiagen) according to the manufacturer's protocol. To remove potentially contaminating DNA, samples were digested with RQ1 DNase (Promega). First strand cDNA synthesis was then performed using Moloney murine leukemia virus reverse transcriptase (Promega) and

oligo(dT)15 primer according to the manufacturer's instruction. cDNA samples were stored at -20°C until usage and were 1:50 diluted in H₂O for quantitative real-time PCR (qPCR) analysis. qPCR reactions contained 8 µL SYBR Green PCR Master Mix, 1.6 µL each reverse and forward primer (10 µM; see Supplementary Table 1, for a list of primes) and 4.8 µL 1:50 cDNA template. Amplification was performed in a 7500 Fast Real-Time PCR system (Applied Biosystems). UBIQUITIN 5 (UBQ5; At3g62250) was used to normalize gene expression with the delta-delta Ct method (Livak and Schmittgen 2001).

Determination of chlorophyll

Chlorophyll was extracted from frozen homogenized leaf material into acetone as described (Christ et al. 2012) and quantified photospectroscopically (Strain et al. 1971). A SAPD-502Plus meter (Minolta) was used for nondestructive measurements of Chl levels of the same wild type leaves over their entire lifespan.

Spectroscopic data of *At*-NCC-5

UV/Vis λ_{\max} ($c = 3.3 \times 10^{-5}$ M, MeOH, ϵ_{rel}) = 312 (1.00), 240 sh (1.28), 216 (1.73) (Supplementary Fig. 5). **CD**. $\lambda_{\text{min/max}}$ ($c = 3.3 \times 10^{-5}$ M, MeOH, $\Delta\epsilon$) = 313 (1.7), 282 (-5.1), 250 sh (1.5), 228 (5.9).

¹H-NMR (600 MHz, CD₃OD, 283 K). δ [ppm] = 0.98 (t, H₃C-3²), 1.86 (s, H₃C-2¹), 1.91 (s, H₃C-13¹), 2.09 (s, H₃C-7¹), 2.11 (s, H₃C-2¹), 2.37 (m, H₂C-12²), 2.39 (m, H_AC-3¹), 2.42 (m, H_BC-3¹), 2.50 (dd, $J = 14.6/9.2$ Hz, H_AC-15), 2.67 (m, H_AC-12¹), 2.73 (m, H_BC-12¹), 2.78 (dd, $J = 14.6/5.7$ Hz, H_BC-15), 3.89 (s, H₂C-5), 4.06 (m, HC-16), 4.82 (s, HC-10), 5.34 (dd, $J = 11.7/2.1$ Hz, H_AC-18²), 6.10 (dd, $J = 17.8/2.1$ Hz, H_BC-18²), 6.44 (dd, $J = 17.8/11.6$ Hz, HC-18¹), 9.33 (s, HC-20) (Supplementary Fig. 6).

¹³C-NMR (CD₃OD, 283 K): δ [ppm] = 8.5 (2¹), 9.2 (13¹), 9.2 (7¹), 12.3 (17¹), 15.0 (3²), 17.3 (3¹), 21.5 (12¹), 23.3 (5), 30.3 (15), 37.9 (10), 38.7 (12²), 61.5 (16), 138.1 (4), 71.7 (8⁵), 111.9 (7), 115.4 (13), 118.6 (18²), 119.6 (12), 123.6 (14), 125.5 (8), 126.0 (18¹), 126.5 (11), 128.5 (18), 129.0 (1), 132.9 (6), 134.3 (2), 157.0 (17), 162.1 (9), 174.5 (19), 176.6 (12³), 177.1 (20), 180.1 (8³).

ESI-MS m/z (% ion type) = 675.1 (18, [M-H+Na+K]⁺); 653.1 (98, [M+K]⁺); 637.1 (49, [M+Na]⁺); 617.1 (19), 616.1 (59), 615.1 (100, C₃₄H₃₉N₄O₇⁺, [M+H]⁺), 597.2 (16, [M-H₂O+H]⁺); 593.3 (12, [M-CO₂+Na]⁺); 571.1 (14, [M-CO₂+H]⁺); 492.0 (4, [M-ring D+H]⁺); 474.2 (4, [M-ring D-H₂O+H]⁺); 448.1 (7, [M-CO₂-ring D+H]⁺) (Supplementary Fig. 7).

Results

Analysis of phyllobilins in naturally senescent yellow leaves of wild type *Arabidopsis*

In the extract of individual naturally senescent yellow wild type leaves of *Arabidopsis* eight colorless PBs were detected by HPLC-UV/Vis (Supplementary Fig. 1). An additional yellow fraction was tentatively assigned the structure of a dioxobilin-type yellow Chl catabolite (DYCC) on the basis of its UV/Vis-properties and HPLC/MS data (Li et al. 2019) (Supplementary Fig. 2). All eight colorless PBs were identical with known PBs from wild type *Arabidopsis* leaves that were induced to senesce by storage in darkness for 7 d (Christ et al. 2013; Süßenbacher et al. 2015b). As found in dark-senesced leaves, the naturally de-greened leaves contained *At*-DNCC-33 as the major fraction, and smaller amounts of the colorless PBs *At*-NCC-1, *At-mes16*-4HM-DNCC-44 (= *At*-NDCC-2), *At*-NCC-2, *At*-4HM-DNCC-41, *At*-2HM-*iso*-DNCC-43, *At*-NCC-44 and *At*-NCC-5. (see Supplementary Fig. 1 for HPL chromatograms and Supplementary Fig. 2 for UV/Vis- and MS-spectra).

Chlorophyll quantification in leaves #6 and #8 of wild type *Arabidopsis*

Nondestructive determination of Chl using a SPAD meter indicated that leaf #6 (considered “juvenile”) (Farmer et al. 2013) and leaf #8, i.e. leaves that have been used repeatedly in the past for the analysis of leaf developmental processes in *Arabidopsis* (Baerenfaller et al. 2012; Donnelly et al. 1999), showed no obvious net loss of Chl before 56 DAS and 63 DAS, respectively (Fig. 2B). In addition, extracts of each three representative green leaves #6 and #8 of wild type *Arabidopsis*, sampled at the indicated times were analyzed UV/Vis-spectroscopically (Fig. 2A). These measurements confirmed that at the sampling times used here, the leaves showed no net loss of Chl, i.e. were in a pre-senescent stage.

Analysis of phyllobilins in green leaves of wild type *Arabidopsis*

Three representatives each of the green leaves #6 and #8 of wild type (Col-0) *Arabidopsis*, sampled at the standardized times, were analyzed. They all contained a set of three major colorless fractions of PBs, according to HPLC analysis (Fig. 3A, Supplementary Fig. 3), besides several very minor tentative PB fractions. Based on UV/Vis-spectral and mass spectrometric properties (Fig. 3B), the three PBs were classified (in the order of decreasing polarity) as a DNCC and as two NCCs. The polar *At*-DNCC-33 was identified by its HPLC retention time ($r_t = 33$ min) and m/z ($[M+H]^+$) = 619) with the known *At*-DNCC-33 (see Fig. 5) (Christ et al. 2013; Süßenbacher et al. 2015b). The NCCs at $r_t = 36$ min (*At*-NCC-36) and

m/z ($[M+H]^+$) = 793 and at r_t = 44 min (*At*-NCC-44) and m/z ($[M+H]^+$) = 807 were identified with known polar *At*-NCCs from senescent leaves of wild type *Arabidopsis*, earlier named *At*-NCC-1 and *At*-NCC-44, respectively (Christ et al. 2013; Pružinská et al. 2005). *At*-NCC-36 (= *At*-NCC-1) and *At*-NCC-44 represent O3³-glucopyranosylated type-I PBs (see Fig. 5), in which the presence of a free carboxylic acid or a methyl ester group at C8², respectively, induces their different polarity. The relatively abundant sugar-free type-II PB *At*-DNCC-33 is the major PB in senescent wild type *Arabidopsis* leaves (Christ et al. 2013).

Hence, the three PBs detected in green wild type *Arabidopsis* leaves were also found in naturally de-greened, yellow leaves of wild type *Arabidopsis*, as reported here, and are all known from earlier work on Chl breakdown in dark-induced senescent wild type *Arabidopsis* leaves (Christ et al. 2013; Pružinská et al. 2005). They all display functional groups consistent with the PAO/phyllobilin pathway, featuring the activities of the hydroxylase TIC55 (Hauenstein et al. 2016), the deformylase CYP89A9 (Christ et al. 2013), the methyl esterase MES16 (Christ et al. 2012) and of a still unidentified glucosyltransferase, a type of activity during Chl breakdown indicated to be relevant in many plant species (Hörtensteiner 2013; Hörtensteiner and Kräutler 2011), in which various glucosylated PBs occur (Erhart et al. 2016; Mühlecker and Kräutler 1996; Scherl et al. 2016).

Analysis of phyllobilins in green leaves of chlorophyll catabolic mutants of *Arabidopsis*

As was done for the wild type, three representative green leaves #6 and #8 were sampled at the standardized times for *mes16-1*, *cyp89a9-1*, the *mes-1/cyp89a9-1* double mutant and for *tic55-3*. Extracts of green *mes16-1* leaves contained a set of three major colorless fractions of PBs, according to an HPLC analysis (Fig. 4, Supplementary Fig. 3). These PBs were classified as an FCC, a DNCC and as an NCC, based on their UV/Vis-spectral and mass spectrometric data from LC/MS experiments (Supplementary Fig. 4). By their HPLC retention time at r_t = 40 min (*At*-FCC-40) and m/z ($[M+H]^+$) = 807, at r_t = 42 min (*At*-DNCC-42) and m/z ($[M+H]^+$) = 633, and at r_t = 44 min (*At*-NCC-44) and m/z ($[M+H]^+$) = 807 (for chemical formulae see Fig. 5) were all identified with PBs known from investigations of senescent leaves of *mes16-1* (Christ et al. 2012; Pružinská et al. 2005; Süssenbacher et al. 2014). The O3³-glucopyranosylated fluorescent *At*-FCC-40, its non-fluorescent isomer *At*-NCC-44 and the sugar-free *At*-DNCC-42 were identified (earlier named *mes16*-FCC-1, *At*-NCC-4 and *At-mes16*-DNCC-38, respectively) (Christ et al. 2012; Süssenbacher et al. 2014). These three PBs display functional groups consistent with the known PAO/phyllobilin pathway in yellow, senescent leaves of the *mes16-1* mutant of *Arabidopsis* featuring all PB-

modifying activities present in wild type, but lacking MES16 (Fig. 5).

Extracts of *cyp89a9-1* contained two major colorless PBs (Fig. 4, Supplementary Fig. 3). Both PBs could be classified as NCCs with $[M+H]^+$ pseudo-molecular ions occurring at m/z 793 and at m/z 807, respectively, as shown by their UV/Vis- and mass spectra in LC/MS experiments (Supplementary Fig. 4). The HPLC retention times at $r_t = 36$ min (of *At*-NCC-36) and at $r_t = 44$ min (of *At*-NCC-44) were the same as those of the two NCCs identified here in green leaves of wild type *Arabidopsis* (Fig. 3, for chemical formulae see Fig. 5), two glucosylated NCCs, described earlier as *At*-NCC-1 and its less polar methyl ester *At*-NCC-4 (Christ et al. 2013; Pružinská et al. 2005). Both of these PBs are of type I, consistent with the absence of the activity of CYP89A9, and represent major PBs in extracts of yellow, senescent leaves of *cyp89a9* mutants of *Arabidopsis* (Christ et al. 2013) (Fig. 5). Hence, these two type-I PBs display functional groups consistent with a PAO/phyllobilin pathway featuring the activity TIC55, MES16 and the ubiquitous glycosyltransferase (Hörtensteiner 2013; Hörtensteiner and Kräutler 2011).

Extracts of the *cyp89a9-1/mes16-1* double mutant contained two major colorless PBs (Fig. 4, Supplementary Fig. 3). One of them could be classified as an FCC, the other as an NCC based on their UV/Vis- and mass spectra, detected in LC/MS experiments (Supplementary Fig. 4). For both PBs $[M+H]^+$ pseudo-molecular ions were observed at m/z 807. The HPLC retention time of the FCC at 40 min (*At*-FCC-40) and of the NCC at 44 min (*At*-NCC-44) (for chemical formulae see Fig. 5) were consistent with the known glucosylated *mes16*-FCC-1 and its slightly less polar isomer *At*-NCC-44 (Pružinská et al. 2005). Both of these PBs are of type I and feature an O8⁴-methyl ester function, consistent with the absence of the activities of both, CYP89A9 and MES16 (see Fig. 5).

In extracts of *tic55-3* one major colorless PB (*At*-HM-DNCC-41) was detected at 254 nm (Fig. 4 Supplementary Fig. 3). This PB could be classified as a hydroxymethylated DNCC based on its UV/Vis-spectral and mass spectrometric properties (Supplementary Fig. 4). The $[M+H]^+$ pseudo-molecular ion was detected at m/z 633 by LC/MS analysis. It was identified by its common HPLC retention time with an authentic sample of *At*-4HM-DNCC-41 from senescent wild type *Arabidopsis* leaves (Süssenbacher et al. 2015b) (for chemical formulae see Fig. 5). This PB of type II displays a free carboxylic acid function at C8² and it carries an ethyl, a methyl and a hydroxymethyl group at ring A, consistent features of the strikingly ‘hydroxymethylated’ Chl catabolites derived from *p*FCC (Süssenbacher et al. 2015b) in the absence of the activity of the hydroxylase TIC55 (Hauenstein et al. 2016) (Fig. 5).

Abundance of phylobilins in green leaves of *Arabidopsis*

The normalized HPLC responses at 254 nm (HPLC system I, see Materials and Methods and SI for details on calibration and numerical analysis) of extracts of three separate leaf samples # 6 each of wild type *Arabidopsis*, of *mes16-1*, *cyp89A9*, of *mes16-1/cyp89A9* and of *tic55* (see Figs. 3 and 4) were quantified (Supplementary Tables 2-6), in order to determine the amounts of PBs (in nmol/g leaf weight) present (see Fig. 6). The HPLC responses at 250 nm or at 320 nm (HPLC system II, see Materials and Methods) of extracts of three separate leaf samples # 8 each of wild type *Arabidopsis*, of *mes16-1*, *cyp89A9*, of *mes16-1/cyp89A9* and of *tic55* (Supplementary Fig. 4) were likewise normalized, allowing for a quantitative determination of the PBs (Supplementary Tables 7-11). In all lines and in both leaf #6 and #8, PB abundancies increased by a factor of roughly three in the course of the experiments, i.e. when leaf samples d0-l or d1-d were compared with samples d7-l and d8-d, respectively, indicating some progressive accumulation of PBs in green leaves during the course of their development. In line with this, leaf #8, i.e. the ‘younger’ leaf, contained reproducibly smaller amounts of PBs than leaf #6, i.e. the ‘older’ leaf. Furthermore, the amounts of the PBs tended to increase slightly in both leaf #6 and #8 during the dark periods, suggesting an increased activity of essential processes of the PAO/phylobilin pathway during the 16 h-dark periods. Maximal overall abundancies of the analyzed major PBs did not exceed 2.2 and 7.8 nmol PB per g fresh weight for leaf #8 and #6, respectively (Fig. 6). Thus, compared to the amounts of Chl present at these stages of leaf development (roughly 1.25 $\mu\text{mol/g}$, see Fig. 2A), PBs accounted for less than 1% of the Chl. Interestingly, the overall amounts of the PBs detected in wild type *Arabidopsis* leaves and in each of the four CCE mutants differed only marginally (Fig. 6).

Chlorophyll catabolic gene expression analysis

To investigate the possibility of a transcriptional regulation of CCE genes during the course of the experiment, transcript abundance in leaf #8 of the wild type was analyzed by quantitative real time PCR (Fig. 7). Most of the genes that are known to be transcriptionally up-regulated during leaf senescence, i.e. *NYC1*, *SGR1*, *SGR2*, *PAO*, *MES16* and *CYP89A9* (Christ et al. 2012; Christ et al. 2013; Kusaba et al. 2007; Pružinská et al. 2005; Sakuraba et al. 2014), exhibited an increase in expression between d0-l and d7-l. This indicated that already at this early (green) stage of development of leaf #8, CCE gene expression progressively increases, correlating with the increase of the amounts of PBs between the sampling times around 42 DAS (d0-l and d1-d) and 49 DAS (d7-l and d8-d) (Fig. 6). Surprisingly, a comparison of the

expression of CCE genes between end-of-day (d0-l and d7-l, respectively) and end-of-night (d1-d and d8-d, respectively) time points, demonstrated that several genes, i.e. *NYC1*, *SGR2*, *PPH*, *PAO*, *RCCR* and *TIC55*, were down-regulated during the dark phase, indicating a light-dependent regulation comparable to many photosynthetic genes (Bläsing et al. 2005). An exception was MES16, whose expression was massively up-regulated during the dark phase (Fig. 7).

Discussion

When leaves of higher plants become senescent and de-green, Chl is broken down via the common and tightly regulated PAO/phyllobilin pathway, as established by the characterization of PBs and by the identification of key CCEs (Kräutler 2016; Kuai et al. 2018). Chl breakdown in senescent leaves of *Arabidopsis thaliana* plants has been the subject of a range of systematic studies (for a review, see Tanaka et al., 2011). In fact, two important branches of the PAO/phyllobilin pathway operate in such leaves, furnishing 1-formyl-19-oxobilin type (or type-I) PBs, as well as 1,19-dioxobilin-type (or type-II) PBs (Christ et al. 2013; Kräutler 2016). Reported here is a first fundamental investigation of Chl breakdown in green non- or pre-senescent leaves of *Arabidopsis*. Leaves of wild type plants and of plants with mutations in PB-modifying enzymes, i.e. *TIC55*, *CYP89A9* and *MES16* and a *CYP89A9/MES16* double mutant were analyzed in parallel. These mutations do not affect the growth of *Arabidopsis*, i.e. have no obvious effect on plant development and senescence. (Christ et al. 2016; Christ et al. 2012; Christ et al. 2013; Hauenstein et al. 2016).

Consistent with the visible persistence of green color of leaves #6 and #8 during the time of investigation between 42 and 49 DAS (see Fig. 2), the total amount of Chl varied insignificantly and a net decrease of the Chl content was only detected after about 52 and 55 DAS for leaves #6 and #8, respectively (Fig. 2B). Nevertheless, in the extracts of such leaves, small amounts of specific colorless Chl catabolites (PBs) could be detected based on their UV/Vis-spectroscopic, HPLC chromatographic and mass spectrometric properties. By comparison of the spectral data with those of known PBs from *Arabidopsis*, the observed (more abundant) Chl catabolites were identified unambiguously. The PBs detected showed the structural modifications known from corresponding yellow, senescent *Arabidopsis* leaves. Hence, in green wild type *Arabidopsis* leaves, three colorless PBs were found (*At*-DNCC-33, *At*-NCC-36 and *At*-NCC-44, see Fig. 3) whose structures required the activity of all three CCEs analyzed (*CYP89A9*, *MES16* and *TIC55*). Correspondingly, in leaves of the mutants

(up to) three main colorless PBs were identified and quantified, the structures of which were fully consistent with the absence of the specific activity of the deleted CCEs. Thus, the PAO/phyllobilin pathway of Chl breakdown, known from senescent leaves, is also indicated to be active in green leaves.

Indeed, in all green leaves investigated here could PBs clearly be detected and identified, even though the major PB fractions came up for less than 1% of the Chl still present. Since the abundance of PBs closely correlates to the amounts of Chl degraded in senescent *Arabidopsis* leaves (Christ et al. 2013), these results indicate that only a minor fraction of Chl is at all degraded in green leaves. Occasionally, the amounts of PBs found in individual leaf extracts showed a significant spread, in particular in leaves of the time advanced sets d7-*l* and d8-*d* of leaves #8, representing leaves harvested at 48 or 49 DAS (Figs. 2 and 6). On the basis of the structure and quantity of the PBs analyzed here in the extracts of the green *Arabidopsis* leaves, several general trends were observed with respect to the PB accumulation. Thus, (i) type-II PBs dominated in green leaves of wild type leaves and in mutants with active CYP89A9, but were absent in CYP89A9 mutants; (ii) polar PBs with two carboxylic acid functions were not observed in MES16 mutants; (iii) the PBs observed in the TIC55 mutant lacked the 3²-OH group. These three observations confirm PB occurrence in green *Arabidopsis* leaves consistent with the known PAO/phyllobilin pathway of Chl degradation, and with the exclusive catabolic relevance of the known CCEs (Hörtensteiner and Kräutler 2011; Kuai et al. 2018).

The amounts of PBs in green leaves of *Arabidopsis* were determined by calibrated HPLC analyses of extracts of leaf samples #6 and #8 of each line (Fig. 4, Supplementary Tables 2-11). The overall amounts of the PBs detected in wild type *Arabidopsis* leaves and in each of the four CCE mutants differed only slightly. Maximal overall amounts of the analyzed major PBs did not exceed 2.2 or 7.8 nmol PB per g fresh weight for leaves #8 and #6, respectively. Compared to the amounts of Chl present at these stages of leaf development (roughly 1.25 μ mol/g; Fig. 2), PBs accounted for less than 1% of the Chl. Hence, several general trends were, furthermore, observed regarding the accumulated PBs in the green *Arabidopsis* leaves: (i) independent of the genotype, the total amounts of PBs increased by a factor of roughly three in the course of the experiments, i.e., when leaf samples d0-*l* or d1-*d* were compared with those in samples d7-*l* and d8-*d*, respectively; (ii) the total amounts of PBs were less by a factor of up to about three in the younger leaves #8 than in the older leaves #6 and (iii) the total amounts of PBs were similar after each of the light and the dark periods in both types of leaves (#6 and #8), with only a slight tendency to increase during the dark periods.

The first two observations suggest accumulation of PBs with time and/or the effect of a transition into a senescent leaf stage (despite the absence of visual de-greening) at the later leaf sampling times. In *Arabidopsis*, leaf senescence is dynamic with spatial and temporal variability; thus, defining a clear ‘senescence start point’ is difficult (Breeze et al. 2011; Miao and Zentgraf 2007). The third observation suggests a multi-factorial dependence of overall Chl breakdown, including light-dark and circadian rhythms and PS II repair (see below).

In line with the variation in the levels of PBs, genes encoding CCEs that are known to be transcriptionally up-regulated during senescence, i.e. *NYC1* (Kusaba et al. 2007), *SGR1* (Sakuraba et al. 2014), *SGR2* (Wu et al. 2016), *PAO* (Pružinská et al. 2005), *MES16* (Christ et al. 2012) and *CYP89A9* (Christ et al. 2013) generally also increased expression from d0-*l*/d1-*d* to d7-*l*/d8-*d*. This corroborates previous analysis of transcriptional regulation of CCE genes (Breeze et al. 2011) that demonstrated an age-dependent increase of *NYC1*, *SGR1*, *SGR2*, *PAO* expression before visible senescence. Surprisingly, there was no strong coupling of gene expression to the light/dark cycle, suggesting that the increase of CCE gene expression seen from one week to the next was rather the results of a developmental process than a dark phase-induced phenomenon. The exception to this was *MES16* whose expression was massively increased at the end of the night time points, d1-*d* and d8-*d*, as compared to the end of day sampling points, d0-*l* and d7-*l*. Besides demethylation of PBs at the C8² position, *MES16* has been demonstrated to hydrolyze indole acetic acid methyl ester, an inactive form of auxin, in vitro (Christ et al. 2012; Li and Pu 2016). Very recently, auxin methylation has been shown to be required for auxin gradient formation within the *Arabidopsis* hypocotyl (Abbas et al. 2018), but whether *MES16* may be involved in auxin metabolism in vivo remains to be shown.

The unprecedented detection of PBs in green leaves indicates occurrence of Chl breakdown in the absence of visible leaf senescence. The observed PBs and their deduced metabolic formation are consistent with the general PAO/phyllobilin pathway, in which Pheide *a* represents the last green tetrapyrrole stage, preceding the key ring cleavage reaction catalyzed by PAO (Pružinská et al. 2003; Pružinská et al. 2005). Along this pathway, Pheide *a* and phytol are generated in senescent leaves from Phein *a* by PPH (Schelbert et al. 2009). Phein *a* is produced from Chl *a* by removal of the Mg-ion, a process that is catalyzed by SGR1 and SGR2, which both have been shown to be relevant for senescence-related Chl breakdown (Shimoda et al. 2016). Loss of the Mg-ion from Chl *a* may also occur by a very slow spontaneous process in aqueous solution (Saga and Tamiaki 2012). Both, PPH and SGRs are selective for *a*-type Chl pigments (see Figs. 1 and 8).

In green non-senescent leaves loss of Chl is minimal and Chl breakdown has, so far, not been documented (Breeze et al. 2011; Ougham et al. 2008), but substantial Chl turnover takes place (Beisel et al. 2010; Lin et al. 2016). Indeed, as proposed here, Chl turnover appears to entertain a remarkable relationship with Chl breakdown in green leaves. The rapid repair of PS II core proteins (Komenda et al. 2012) not only sets free the protein-bound ‘major’ photosynthetic pigment, Chl *a*, but also the ‘minor’ analogue, Phein *a*, i.e. the first electron acceptor after P680 (Vass and Cser 2009). In association with the PS II repair cycle in *Arabidopsis*, a pathway has been proposed that recycles Chl *a* through dephytylation to Chlide *a* by CLD1, followed by Chl *a* re-synthesis by CHLG (Lin et al. 2016). Strikingly, the also liberated Phein *a* (which is present in the PS II core in a 1:2 ratio with Chl *a*) has received little attention and a corresponding biochemical mechanism for its recycling lacks experimental support. Whereas Phein *a* is prone to loss of its phytol side chain causing formation of Pheide *a* (by PPH or, possibly, by CLD1) (Lin et al. 2016; Schelbert et al. 2009), no evidence exists for the reverse process, i.e. re-synthesis of Mg-free Phein *a* from Pheide *a*. CHLG does not accept metal-free porphyrins, such as Pheide *a*, as substrate (Helfrich et al. 1994). Likewise, incorporation of a Mg-ion into Phein *a* or other metal-free Chl derivative is unknown, and rather unlikely. Instead, the highly regulated and still incompletely characterized Mg-incorporation into the porphyrinoid precursor protoporphyrin IX by Mg-chelatase (Mochizuki et al. 2010) has evolved as the single common step in the biosynthesis of the Chls and bacteriochlorophylls from metal-free porphyrinoids (Chew and Bryant 2007; Heyes and Hunter 2008). Phein *a*, set free during PS II repair and the associated Chl turnover may, hence, suffer effective dephytylation to Pheide *a*, to be channeled into the PAO/phyllobilin pathway for further degradation, although an, at least partial, direct re-incorporation of Phein *a* during PS II repair cannot be ruled out. However, in order to avoid photodynamic damage, this would require temporary storage of Phein *a* outside D1, i.e. within a pigment-binding protein whose nature remains to be determined. Our experimental data are consistent with a scenario of Phein *a* degradation (in particular in the context of the repair of PS II and the associated turnover of photosynthetic pigments) in green, non-senescent leaves of *Arabidopsis*. Phein *a*, the second essential porphyrinoid component of PS II, represents an effective source of Pheide *a*, which is the key phototoxic target for the controlled degradation by the PAO/phyllobilin pathway of Chl breakdown (see Fig. 8). Hence, we propose a second vital role of Chl breakdown in higher plants that has remained invisible in the green, photoactive leaves of the primarily investigated angiosperms. Probably, such a role in the context of the maintenance of photosynthetic activity may already have

contributed to functional photosynthesis in very early stages of the evolution of green plants. Homologs of several CCEs are present in cyanobacteria (Gray et al. 2004; Thomas et al. 2009), but a potential role in Chl breakdown has not yet been demonstrated that would cause ‘de-greening’ of respective photosynthetic organisms, comparable to senescence in higher plants.

As a consequence of the scenario discussed above, PS II turnover would, furthermore, require de novo generation of Phe α for incorporation into new core complexes. The source of PS II-located Phe α , an indispensable component for photosynthesis (Nickelsen and Rengstl 2013), remains elusive (Chen et al. 2019). However, Chl a is unstable, thermodynamically, with respect to spontaneous loss of its central Mg-ion and pH-dependent non-enzymatic conversion into Phe α occurs with remarkable ease in aqueous solutions at ambient temperatures and, thus, may be the path by which the required Phe α for PS II assembly is supplemented (Saga and Tamiaki 2012). Indeed, an SGR1/SGR2/SGRL triple mutant that lacks any known Mg-dechelating activity is not compromised in photosynthesis (Chen et al. 2019). However, metabolic fine tuning would be lost in a scenario of the non-enzymatic production of Phe α . Future experiments using this triple mutant are required to confirm our hypothesis that the PAO/phyllobilin pathway in green leaves is responsible for specific degradation of Phe α , but not Chl a , during PS II repair and the turnover of its associated pigments.

We rationalize the absence of a net loss of Chl and the here reported observation of PBs and CCEs in green non-senescent leaves by a cryptic constitutive form of the common PAO/phyllobilin pathway of Chl breakdown that scavenges phototoxic Phe α . Phe α is liberated in the course of PS II repair as the ‘non-recyclable’ component of Chl turnover and may be available from non-enzymatic loss of Mg from Chl a (Saga and Tamiaki 2012). Furthermore, the presence of PBs in photosynthetically active green leaves is documented here for the first time. The basic structural features of PBs (Kräutler 2016) are remarkably related to those of heme-derived bilins (Falk 1989), some of which have key functions in photo-regulation (Burgie and Vierstra 2014). Hence, among the Chl-derived bilin-type PBs may be candidates for relevant physiological roles in plants, inviting studies dedicated to unravelling such biological contributions of PBs from Chl breakdown.

Conflict of Interest:

The authors declare that they have no conflict of interest.

References

- Abbas M et al. (2018) Auxin methylation is required for differential growth in *Arabidopsis*. *Proceedings of the National Academy of Sciences, USA* 115:6864-6869. doi:10.1073/pnas.1806565115
- Aro EM, McCaffery S, Anderson JM (1993) Photoinhibition and D1 protein degradation in peas acclimated to different growth irradiances. *Plant Physiol* 103:835-843.
- Baerenfaller K et al. (2012) Systems-based analysis of *Arabidopsis* leaf growth reveals adaptation to water deficit. *Mol Syst Biol* 8:606. doi:10.1038/msb.2012.39
- Beisel KG, Jahnke S, Hofmann D, Köppchen S, Schurr U, Matsubara S (2010) Continuous turnover of carotenes and chlorophyll *a* in mature leaves of *Arabidopsis* revealed by ¹⁴CO₂ pulse-chase labeling. *Plant Physiol* 152:2188-2199. doi:10.1104/pp.109.151647
- Bläsing OE et al. (2005) Sugars and circadian regulation make major contributions to the global regulation of diurnal gene expression in *Arabidopsis*. *Plant Cell* 17:3257-3281. doi:10.1105/tpc.105.035261
- Breeze E et al. (2011) High-resolution temporal profiling of transcripts during *Arabidopsis* leaf senescence reveals a distinct chronology of processes and regulation. *Plant Cell* 23:873-894. doi:10.1105/tpc.111.083345
- Burgie ES, Vierstra RD (2014) Phytochromes: an atomic perspective on photoactivation and signaling. *Plant Cell* 26:4568-4583. doi:10.1105/tpc.114.131623
- Chen Y, Shimoda Y, Yokono M, Ito H, Tanaka A (2019) Mg-dechelataase is involved in the formation of photosystem II but not in chlorophyll degradation in *Chlamydomonas reinhardtii*. *Plant J* 97:1022-1031. doi: 10.1111/tpj.14174
- Chew AG, Bryant DA (2007) Chlorophyll biosynthesis in bacteria: the origins of structural and functional diversity. *Annu Rev Microbiol* 61:113-129. doi:10.1146/annurev.micro.61.080706.093242
- Christ B, Egert A, Süßenbacher I, Kräutler B, Bartels D, Peters S, Hörtensteiner S (2014) Water deficit induces chlorophyll degradation via the ‘PAO/phyllobilin’ pathway in leaves of homoio- (*Craterostigma pumilum*) and poikilochlorophyllous (*Xerophyta viscosa*) resurrection plants. *Plant Cell Environ* 37:2521-2531.
- Christ B, Hauenstein M, Hörtensteiner S (2016) A liquid chromatography-mass spectrometry platform for the analysis of phyllobilins, the major degradation products of chlorophyll in *Arabidopsis thaliana*. *Plant J* 88:505-518. doi:10.1111/tpj.13253

- Christ B, Schelbert S, Aubry S, Süßenbacher I, Müller T, Kräutler B, Hörtensteiner S (2012) MES16, a member of the methylesterase protein family, specifically demethylates fluorescent chlorophyll catabolites during chlorophyll breakdown in *Arabidopsis*. *Plant Physiol* 158:628-641. doi:10.1104/pp.111.188870
- Christ B et al. (2013) Cytochrome P450 CYP89A9 is involved in the formation of major chlorophyll catabolites during leaf senescence in *Arabidopsis*. *Plant Cell* 25:1868-1880. doi:10.1105/tpc.113.112151
- Curty C, Engel N (1996) Detection, isolation and structure elucidation of a chlorophyll *a* catabolite from autumnal senescent leaves of *Cercidiphyllum japonicum*. *Phytochemistry* 42:1531-1536. doi:10.1016/0031-9422(96)00155-0
- Donnelly PM, Bonetta D, Tsukaya H, Dengler RE, Dengler NG (1999) Cell cycling and cell enlargement in developing leaves of *Arabidopsis*. *Dev Biol* 215:407-419. doi:10.1006/dbio.1999.9443
- Erhart T et al. (2018) Novel types of hypermodified fluorescent phyllobilins from breakdown of chlorophyll in senescent leaves of grapevine (*Vitis vinifera*). *Chem-Eur J* 24:17268-17279. doi:10.1002/chem.201803128
- Erhart T et al. (2016) Chlorophyll catabolites in senescent leaves of the plum tree (*Prunus domestica*). *Chem Biodivers* 13:1441-1453. doi:10.1002/cbdv.201600181
- Falk H (1989) Chemistry of Linear Oligopyrroles and Bile Pigments. Springer, Wien
- Farmer E, Mousavi S, Lenglet A (2013) Leaf numbering for experiments on long distance signalling in *Arabidopsis*. *Protocol Exchange*:10.1038/protex.2013.1071. doi:10.1038/protex.2013.071
- Feierabend J, Dehne S (1996) Fate of the porphyrin cofactors during the light-dependent turnover of catalase and of the photosystem II reaction-center protein D1 in mature rye leaves. *Planta* 198:413-422. doi:10.1007/Bf00620058
- Gray J, Wardzala E, Yang M, Reinbothe S, Haller S, Pauli F (2004) A small family of LLS1-related non-heme oxygenases in plants with an origin amongst oxygenic photosynthesizers. *Plant Mol Biol* 54:39-54. doi:10.1023/B:PLAN.0000028766.61559.4c
- Grumbach KH, Lichtenthaler HK, Erismann KH (1978) Incorporation of $^{14}\text{CO}_2$ in photosynthetic pigments of *Chlorella pyrenoidosa*. *Planta* 140:37-43. doi:10.1007/BF00389377
- Hauenstein M, Christ B, Das A, Aubry S, Hörtensteiner S (2016) A role for TIC55 as a hydroxylase of phyllobilins, the products of chlorophyll breakdown during plant

- senescence. *Plant Cell* 28:2510-2527. doi:10.1105/tpc.16.00630
- Helfrich M, Schoch S, Lempert U, Cmiel E, Rüdiger W (1994) Chlorophyll synthetase cannot synthesize chlorophyll *a'*. *Eur J Biochem* 219:267-275.
- Heyes DJ, Hunter CN (2008) Biosynthesis of chlorophyll and bacteriochlorophyll. In: Warren MJ, Smith AG (eds) *Tetrapyrroles: Birth, life and Death*. Landes Bioscience, Austin, Texas, pp 233-247
- Horie Y, Ito H, Kusaba M, Tanaka R, Tanaka A (2009) Participation of chlorophyll *b* reductase in the initial step of the degradation of light-harvesting chlorophyll *a/b*-protein complexes in *Arabidopsis*. *J Biol Chem* 284:17449-17456. doi:10.1074/jbc.M109.008912
- Hörtensteiner S (2009) Stay-green regulates chlorophyll and chlorophyll-binding protein degradation during senescence. *Trends Plant Sci* 14:155-162. doi:10.1016/j.tplants.2009.01.002
- Hörtensteiner S (2013) Update on the biochemistry of chlorophyll breakdown. *Plant Mol Biol* 82:505-517. doi:10.1007/s11103-012-9940-z
- Hörtensteiner S, Kräutler B (2011) Chlorophyll breakdown in higher plants. *Biochim Biophys Acta* 1807:977-988. doi:10.1016/j.bbabi.2010.12.007
- Hörtensteiner S, Vicentini F, Matile P (1995) Chlorophyll breakdown in senescent cotyledons of rape, *Brassica napus* L.: enzymatic cleavage of phaeophorbide *a* *in vitro*. *New Phytol* 129:237-246. doi:10.1111/j.1469-8137.1995.tb04293.x
- Komenda J, Sobotka R, Nixon PJ (2012) Assembling and maintaining the photosystem II complex in chloroplasts and cyanobacteria. *Curr Opin Plant Biol* 15:245-251. doi:10.1016/j.pbi.2012.01.017
- Kräutler B (2014) Phyllobilins - the abundant bilin-type tetrapyrrolic catabolites of the green plant pigment chlorophyll. *Chem Soc Rev* 43:6227-6238. doi:10.1039/c4cs00079j
- Kräutler B (2016) Breakdown of chlorophyll in higher plants - Phyllobilins as abundant, yet hardly visible signs of ripening, senescence, and cell death. *Angew Chem Int Ed* 55:4882-4907. doi:10.1002/anie.201508928
- Kräutler B, Hörtensteiner S (2014) Chlorophyll breakdown: chemistry, biochemistry and biology. In: Ferreira GC, Kadish KM, Smith KM, Guillard R (eds) *Handbook of Porphyrin Science - Chlorophyll, Photosynthesis and Bio-inspired Energy*, vol 28. *Handbook of Porphyrin Science*, vol 28. World Scientific Publishing, Singapore, pp 117-185. doi:10.1142/9789814407755_0021
- Kräutler B, Mühlecker W, Anderl M, Gerlach B (1997) Breakdown of chlorophyll: partial

- synthesis of a putative intermediary catabolite. *Helv Chim Acta* 80:1355-1362. doi:10.1002/hlca.19970800504
- Kuai B, Chen J, Hörtensteiner S (2018) The biochemistry and molecular biology of chlorophyll breakdown. *J Exp Bot* 69:751–767. doi:10.1093/jxb/erx322
- Kusaba M et al. (2007) Rice NON-YELLOW COLORING1 is involved in light-harvesting complex II and grana degradation during leaf senescence. *Plant Cell* 19:1362-1375. doi:10.1105/tpc.106.042911
- Kusaba M, Tanaka A, Tanaka R (2013) Stay-green plants: what do they tell us about the molecular mechanism of leaf senescence. *Photosynth Res* 117:221-234. doi:10.1007/s11120-013-9862-x
- Li C, Erhart T, Liu X, Kräutler B (2019) Yellow dioxobilin-type tetrapyrroles from chlorophyll breakdown in higher plants - A new class of colored phyllobilins. *Chem-Eur J*, in press. doi:10.1002/chem.201806038
- Li HM, Pu H (2016) Crystal structure of methylesterase family member 16 (MES16) from *Arabidopsis thaliana*. *Biochem Biophys Res Com* 474:226-231. doi:10.1016/j.bbrc.2016.04.115
- Lim PO, Kim HJ, Nam HG (2007) Leaf senescence. *Annu Rev Plant Biol* 58:115-136. doi:10.1146/annurev.arplant.57.032905.105316
- Lin YP, Lee TY, Tanaka A, Charng YY (2014) Analysis of an *Arabidopsis* heat-sensitive mutant reveals that chlorophyll synthase is involved in reutilization of chlorophyllide during chlorophyll turnover. *Plant J* 80:14-26. doi:10.1111/tpj.12611
- Lin YP, Wu MC, Charng YY (2016) Identification of a chlorophyll dephytylase involved in chlorophyll turnover in *Arabidopsis*. *Plant Cell* 28:2974-2990. doi:10.1105/tpc.16.00478
- Livak KJ, Schmittgen TD (2001) Analysis of relative gene expression data using real-time quantitative PCR and the $2^{-\Delta\Delta C_T}$ method. *Methods* 25:402-408. doi:10.1006/meth.2001.1262
- Matile P, Hörtensteiner S, Thomas H (1999) Chlorophyll degradation. *Annu Rev Plant Physiol Plant Mol Biol* 50:67-95. doi:10.1146/annurev.arplant.50.1.67
- Meguro M, Ito H, Takabayashi A, Tanaka R, Tanaka A (2011) Identification of the 7-hydroxymethyl chlorophyll *a* reductase of the chlorophyll cycle in *Arabidopsis*. *Plant Cell* 23:3442-3453. doi:10.1105/tpc.111.089714
- Miao Y, Zentgraf U (2007) The antagonist function of *Arabidopsis* WRKY53 and ESR/ESP in leaf senescence is modulated by the jasmonic and salicylic acid equilibrium. *Plant*

- Cell 19:819-830. doi:10.1105/tpc.106.042705
- Mittelberger C et al. (2017) Pathogen-induced leaf chlorosis: products of chlorophyll breakdown found in degreened leaves of Phytoplasma-infected apple (*Malus x domestica* Borkh.) and spricot (*Prunus armeniaca* L.) trees relate to the pheophorbide *a* oxygenase/phyllobilin pathway. J Agric Food Chem 65:2651-2660. doi:10.1021/acs.jafc.6b05501
- Mochizuki N et al. (2010) The cell biology of tetrapyrroles: a life and death struggle. Trends Plant Sci 15:488-498. doi:10.1016/j.tplants.2010.05.012
- Mühlecker W, Kräutler B (1996) Breakdown of chlorophyll: constitution of nonfluorescing chlorophyll-catabolites from senescent cotyledons of the dicot rape. Plant Physiol Biochem 34:61-75.
- Mühlecker W, Ongania K-H, Kräutler B, Matile P, Hörtensteiner S (1997) Tracking down chlorophyll breakdown in plants: elucidation of the constitution of a 'fluorescent' chlorophyll catabolite. Angew Chem Int Ed Engl 36:401-404. doi:10.1002/anie.199704011
- Nickelsen J, Rengstl B (2013) Photosystem II assembly: from cyanobacteria to plants. Annu Rev Plant Biol 64:609-635. doi:10.1146/annurev-arplant-050312-120124
- Oberhuber M, Berghold J, Breuker K, Hörtensteiner S, Kräutler B (2003) Breakdown of chlorophyll: a nonenzymatic reaction accounts for the formation of the colorless "nonfluorescent" chlorophyll catabolites. Proc Natl Acad Sci USA 100:6910-6915. doi:10.1073/pnas.1232207100
- Oberhuber M, Berghold J, Kräutler B (2008) Chlorophyll breakdown by a biomimetic route. Angew Chem Int Ed 47:3057-3061. doi:10.1002/anie.200705330
- Ougham H, Hörtensteiner S, Armstead I, Donnison I, King I, Thomas H, Mur L (2008) The control of chlorophyll catabolism and the status of yellowing as a biomarker of leaf senescence. Plant Biol 10 (Suppl. 1):4-14. doi:10.1111/j.1438-8677.2008.00081.x
- Perkins HJ, Roberts DWA (1963) On chlorophyll turnover in monocotyledons and dicotyledons. Can J Bot 41:221-226.
- Pružinská A, Anders I, Tanner G, Roca M, Hörtensteiner S (2003) Chlorophyll breakdown: pheophorbide *a* oxygenase is a Rieske-type iron-sulfur protein, encoded by the *accelerated cell death 1* gene. Proc Natl Acad Sci USA 100:15259-15264. doi:10.1073/pnas.2036571100
- Pružinská A et al. (2005) Chlorophyll breakdown in senescent Arabidopsis leaves: characterization of chlorophyll catabolites and of chlorophyll catabolic enzymes

- involved in the degreening reaction. *Plant Physiol* 139:52-63. doi:10.1104/pp.105.065870
- Ren G et al. (2007) Identification of a novel chloroplast protein AtNYE1 regulating chlorophyll degradation during leaf senescence in *Arabidopsis*. *Plant Physiol* 144:1429-1441. doi:10.1104/pp.107.100172
- Riper DM, Owens TG, Falkowsky PG (1979) Chlorophyll turnover in *Skeletonema costatum*, a marine plankton Diatom. *Plant Physiol* 64:49-54.
- Rodoni S et al. (1997) Chlorophyll breakdown in senescent chloroplasts. Cleavage of pheophorbide *a* in two enzymic steps. *Plant Physiol* 115:669-676. doi:10.1104/pp.115.2.669
- Saga Y, Tamiaki H (2012) Demetalation of chlorophyll pigments. *Chem Biodivers* 9:1659-1683. doi:10.1002/cbdv.201100435
- Sakuraba Y, Park SY, Kim YS, Wang SH, Yoo SC, Hörtensteiner S, Paek NC (2014) *Arabidopsis* STAY-GREEN2 is a negative regulator of chlorophyll degradation during leaf senescence. *Mol Plant* 7:1288-1302. doi:10.1093/Mp/Ssu045
- Schelbert S, Aubry S, Burla B, Agne B, Kessler F, Krupinska K, Hörtensteiner S (2009) Pheophytin pheophorbide hydrolase (pheophytinase) is involved in chlorophyll breakdown during leaf senescence in *Arabidopsis*. *Plant Cell* 21:767-785. doi:10.1105/tpc.108.064089
- Scherl M, Müller T, Kreutz CR, Huber RG, Zass E, Liedl KR, Kräutler B (2016) Chlorophyll catabolites in fall leaves of the wych elm tree present a novel glycosylation motif. *Chem-Eur J* 22:9498-9503. doi:10.1002/chem.201601739
- Scheumann V, Schoch S, Rüdiger W (1999) Chlorophyll *b* reduction during senescence of barley seedlings. *Planta* 209:364-370.
- Shimoda Y, Ito H, Tanaka A (2012) Conversion of chlorophyll *b* to chlorophyll *a* precedes magnesium dechelation for protection against necrosis in *Arabidopsis*. *Plant J* 72:501-511. doi:10.1111/j.1365-313X.2012.05095.x
- Shimoda Y, Ito H, Tanaka A (2016) *Arabidopsis* STAY-GREEN, Mendel's green cotyledon gene, encodes magnesium-dechelataase. *Plant Cell* 28:2147-2160. doi:10.1105/tpc.16.00428
- Strain HH, Cope BT, Svec WA (1971) Analytical procedures for the isolation, identification, estimation and investigation of the chlorophylls. *Methods Enzymol* 23:452-476. doi:10.1016/S0076-6879(71)23118-9
- Süssenbacher I, Christ B, Hörtensteiner S, Kräutler B (2014) Hydroxymethylated

- phyllobilins: A puzzling new feature of the dioxobilin branch of chlorophyll breakdown. *Chem-Eur J* 20:87-92. doi:10.1002/chem.201303398
- Süssenbacher I, Hörtensteiner S, Kräutler B (2015a) A dioxobilin-type fluorescent chlorophyll catabolite as a transient early intermediate of the dioxobilin-branch of chlorophyll breakdown in *Arabidopsis thaliana*. *Angew Chem Int Ed* 54:13777-13781. doi:10.1002/anie.201506299
- Süssenbacher I, Kreutz C, Christ B, Hörtensteiner S, Kräutler B (2015b) Hydroxymethylated dioxobilins in senescent *Arabidopsis thaliana* leaves - sign of a puzzling biosynthetic intermezzo of chlorophyll breakdown. *Chem-Eur J* 21:11664-11670. doi:10.1002/chem.201501489
- Tanaka R, Kobayashi K, Masuda T (2011) Tetrapyrrole metabolism in *Arabidopsis thaliana*. *The Arabidopsis Book* 9:e0145. doi:10.1199/tab.0145
- Theis J, Schroda M (2016) Revisiting the photosystem II repair cycle. *Plant Signal Behav* 11:e1218587. doi:10.1080/15592324.2016.1218587
- Thomas H, Huang L, Young M, Ougham H (2009) Evolution of plant senescence. *BMC Evolution Biol* 9:163. doi:10.1186/1471-2148-9-163
- Vass I, Cser K (2009) Janus-faced charge recombinations in photosystem II photoinhibition. *Trends Plant Sci* 14:200-205. doi:10.1016/j.tplants.2009.01.009
- Vavilin D, Vermaas W (2007) Continuous chlorophyll degradation accompanied by chlorophyllide and phytol reutilization for chlorophyll synthesis in *Synechocystis* sp. PCC 6803. *Biochim Biophys Acta* 1767:920-929. doi:10.1016/j.bbabi.2007.03.010
- Vergeiner C, Banala S, Kräutler B (2013) Chlorophyll breakdown in senescent banana leaves: catabolism reprogrammed for biosynthesis of persistent blue fluorescent tetrapyrroles. *Chem-Eur J* 19:12294-12305. doi:10.1002/chem.201301907
- Wu S et al. (2016) NON-YELLOWING2 (NYE2), a close paralog of NYE1, plays a positive role in chlorophyll degradation in *Arabidopsis*. *Mol Plant* 9:624-627. doi:10.1016/j.molp.2015.12.016
- Wüthrich KL, Bovet L, Hunziker PE, Donnison IS, Hörtensteiner S (2000) Molecular cloning, functional expression and characterisation of RCC reductase involved in chlorophyll catabolism. *Plant J* 21:189-198. doi:10.1046/j.1365-313x.2000.00667.x

Figure legends

Fig. 1. Outline of the ‘early part’ of the common PAO/phyllobilin pathway of Chl breakdown in senescent leaves of wild type *Arabidopsis*. Depicted are enzymes and key 1-formyl-19-oxo-bilin type phyllobilins (PBs), with 1-formyl and 19-oxo groups highlighted blue, and 1,19-dioxo-bilin type (or type-II) PB with red highlighted 1-oxo and 19-oxo groups (see text for abbreviations of tetrapyrroles displayed). NYC1, non-yellow coloring 1 (Chl *b* reductase); NOL, NYC1-like; HCAR, 7¹-hydroxy-Chl *a* reductase; SGR1/SGR2, stay-green proteins 1 and 2 (Mg-dechelatas); PPH, Phein *a* Pheide *a* hydrolase; PAO, Pheide *a* oxygenase; RCCR, RCC reductase; TIC55, translocon at the inner chloroplast envelope 55 (3²-hydroxylase); CYP89A9, cytochrome P450 monooxygenase 89A9 (1-deformylase); MES16, methylesterase 16 (8⁴-hydrolase).

Fig. 2. Wild type *Arabidopsis* development and sampling times. **A.** Plant development of wild type *Arabidopsis* plant [grown with 8 h light (open bar)/16 h dark (closed bar) cycles]; sampling times and Chl values (mean \pm SD of the biological replicates) of leaves #6 and #8 are shown. Note, filled and open circles, refer to leaves #6 and #8, respectively. DAS, days after sowing. **B.** SPAD values as a measure of relative Chl amounts during the course of development of leaves #6 (filled circles) and #8 (open circles). Data are given as mean \pm SE (leaf #6: *n* = 32, 45, 45, 40, 35, 29, 23 and 23 at 34, 39, 41, 45, 48, 52, 55 and 60 DAS, respectively; leaf #8: *n* = 8, 46, 46, 30, 35, 29, 23 and 23 at 34, 39, 41, 45, 48, 52, 55 and 60 DAS, respectively). Arrows indicate the sampling times at 42 (d0-*l*; d1-*d*) and 49 DAS (d7-*l*; d8-*d*).

Fig. 3. Phyllobilins detected in green leaves of wild type *Arabidopsis*. **A.** HPLC detection of phyllobilins (PBs) at 254 nm in extracts of leaves #6 at sampling times d0-*l*, as d1-*d*, as d7-*l* and as d8-*d*. In the extracts of these leaf samples, DNCC-33, NCC-36 and NCC-44 were identified (see Fig. 5, for chemical formulae and nomenclature). **B.** UV- and mass spectral characterization of PBs from green wild type *Arabidopsis* leaf samples #6 (UV-spectra pictured are from leaf samples #6, positive-ion mass spectra from LC/ESI-MS-data from leaf samples d0-*l*).

Fig. 4. Phyllobilins in extracts of green leaves of different mutants of *Arabidopsis*. HPLC analysis (detection at 254 nm) of extracts of leaves #6 at sampling times d0-*l*, d1-*d*, d7-*l* and d8-*d*. **A.** *mes16-1*; **B.** *cyp89a9-1*; **C.** *cyp89a9-1/mes16-1*; **D.** *tic55-3*. See Fig. 5 for chemical

formulae of phyllobilins and Supplementary Fig. 3 for corresponding traces of leaf #8 samples.

Fig. 5. Colorless phyllobilins detected in leaves of Arabidopsis and their proposed formation along the PAO/phyllobilin pathway from *pFCC*. Chemical formulae and abbreviated phenomenological names of the detected seven phyllobilins (PBs) are depicted, as are the enzymes TIC55, CYP89A9, MES16, Glyc (unknown glycosidase) involved in their formation; ISO, non-enzymatic isomerization; 1-oxo and 19-oxo groups of type-II PBs are highlighted red.

Fig. 6. HPLC-based quantification of phyllobilins detected in green leaves of Arabidopsis. Phyllobilins were analyzed by HPLC in extracts of green leaves #6 and #8 of Arabidopsis at the sampling time points d0-*l*, d1-*d*, d7-*l* and d8-*d*. **A**, wild type; **B**, *mes16-1*; **C**, *cyp89a9-1*, **D**, *cyp89a9-1/mes16-1*; **E**, *tic55-3*. For identification of phyllobilins in each line, see Figs. 3 and 4; for details of the quantification, see Materials and Methods and Supplementary Material. Data are mean \pm SD of three replicates.

Fig. 7. CCE gene expression in green leaves of Arabidopsis. Box plot of CCE gene expression in wild type Arabidopsis leaf #8 as analyzed by qPCR using *UBQ5* expression for normalization. For each gene, four time points, i.e. d0-*l* (white), d1-*d* (light gray), d7-*l* (middle gray) and d8-*d* (dark gray) were used and expression was set to 1 for the d0-*l* sampling point. For gene abbreviations see text.

Fig. 8. Models of Chl degradation in senescent and green leaves. In senescent leaves (**top**), Phein *a* is a key intermediate of the PAO/phyllobilin pathway of massive Chl breakdown, by which Chl *a* and Chl *b* are degraded via Pheide *a*, alongside with the degradation of the protein components of the photosystems. In green leaves (**bottom**), small quantities of phyllobilins are formed from Phein *a* via the PAO/phyllobilin pathway of Chl breakdown. Phein *a* may originate mainly from the repair cycle of photosystem II components (D1 protein). Chl *a*, the dominant photoactive cofactor is turned over without net loss, by dephytylation to Chlide *a* by CLD1, and rephytylation to Chl *a* by CHLG. However, Phein *a* is converted to Pheide *a*, which cannot be reconverted to Phein *a*, but is degraded by the PAO/phyllobilin pathway. Key players of these processes are depicted; relative fluxes are indicated by arrow thickness. For abbreviations of genes and enzymes, see text.

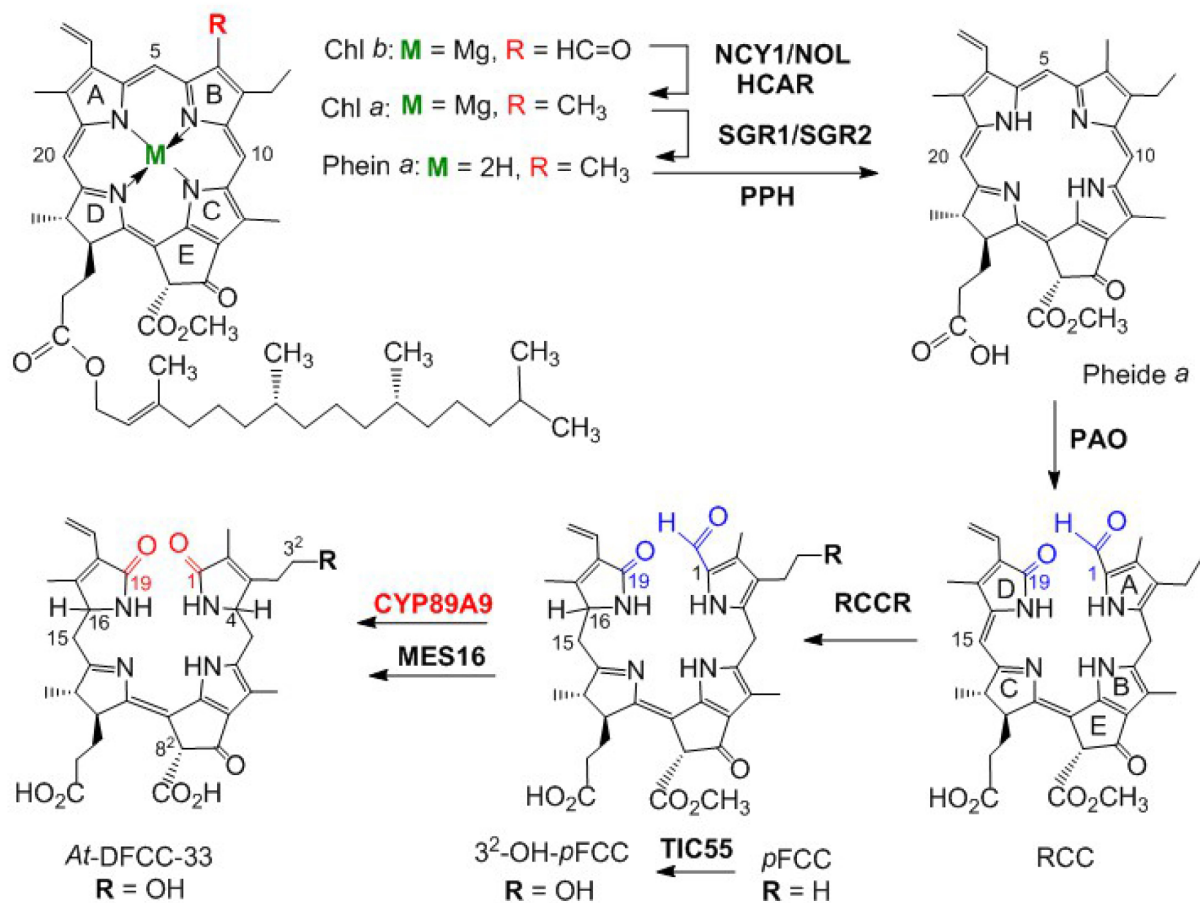


Fig. 1. Outline of the ‘early part’ of the common PAO/phyllobilin pathway of Chl breakdown in senescent leaves of wild type *Arabidopsis*. Depicted are enzymes and key 1-formyl-19-oxo-bilin type phyllobilins (PBs), with 1-formyl and 19-oxo groups highlighted blue, and 1,19-dioxo-bilin type (or type-II) PB with red highlighted 1-oxo and 19-oxo groups (see text for abbreviations of tetrapyrroles displayed). NYC1, non-yellow coloring 1 (Chl *b* reductase); NOL, NYC1-like; HCAR, 7¹-hydroxy-Chl *a* reductase; SGR1/SGR2, stay-green proteins 1 and 2 (Mg-dechelateses); PPH, Pheide *a* Pheide *a* hydrolase; PAO, Pheide *a* oxygenase; RCCR, RCC reductase; TIC55, translocon at the inner chloroplast envelope 55 (3²-hydroxylase); CYP89A9, cytochrome P450 monooxygenase 89A9 (1-deformylase); MES16, methylesterase 16 (8⁴-hydrolase).

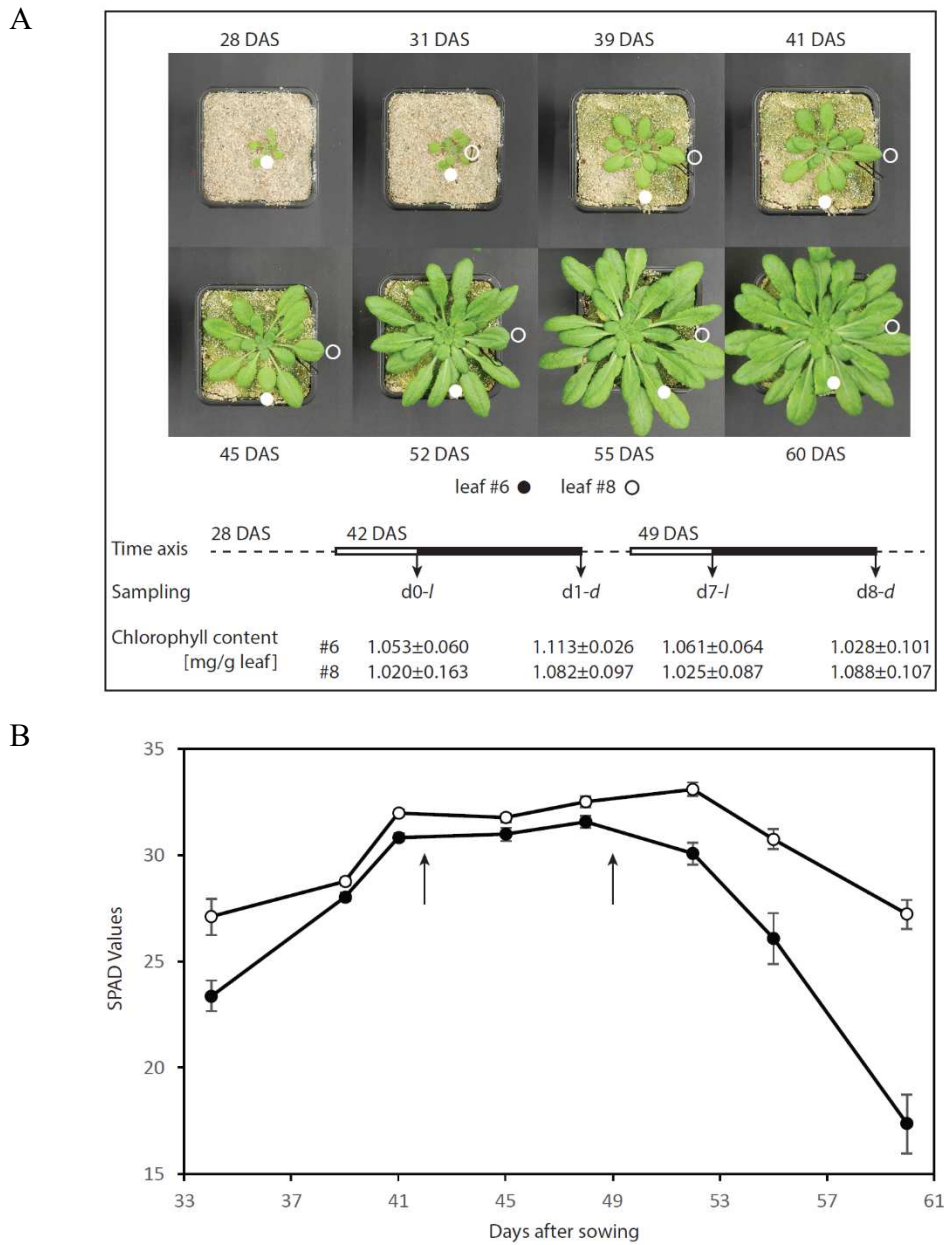


Fig. 2. Wild type *Arabidopsis* development and sampling times. **A.** Plant development of wild type *Arabidopsis* plant [grown with 8 h light (open bar)/16 h dark (closed bar) cycles]; sampling times and Chl values (mean \pm SD of the biological replicates) of leaves #6 and #8 are shown. Note, filled and open circles, refer to leaves #6 and #8, respectively. DAS, days after sowing. **B.** SPAD values as a measure of relative Chl amounts during the course of development of leaves #6 (filled circles) and #8 (open circles). Data are given as mean \pm SE (leaf #6: n = 32, 45, 45, 40, 35, 29, 23 and 23 at 34, 39, 41, 45, 48, 52, 55 and 60 DAS, respectively; leaf #8: n = 8, 46, 46, 30, 35, 29, 23 and 23 at 34, 39, 41, 45, 48, 52, 55 and 60 DAS, respectively). Arrows indicate the sampling times at 42 (d0-l; d1-d) and 49 DAS (d7-l; d8-d).

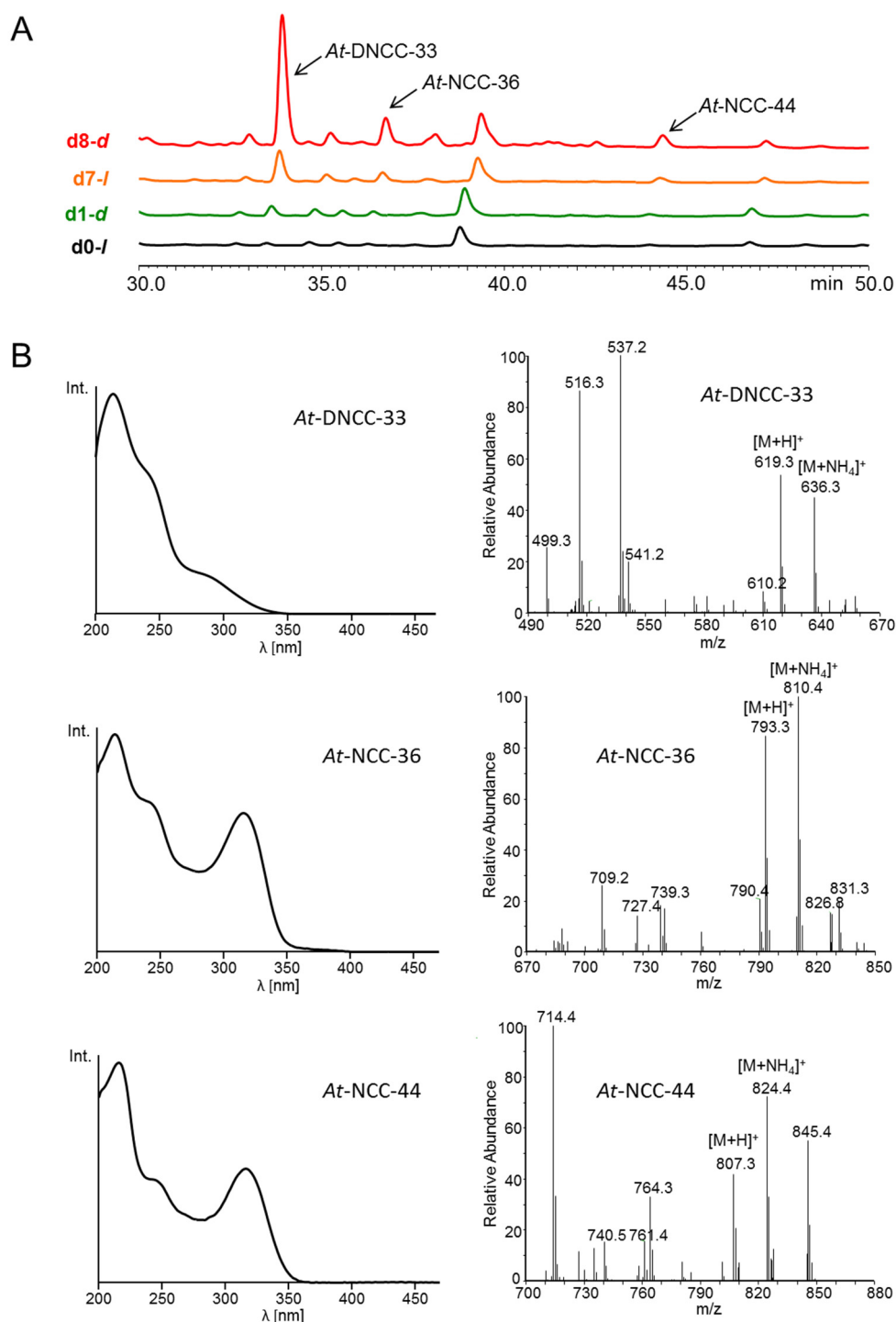


Fig. 3. Phyllobilins detected in green leaves of wild type Arabidopsis. **A.** HPLC detection of phyllobilins (PBs) at 254 nm in extracts of leaves #6 at sampling times d0-l, as d1-d, as d7-l and as d8-d. In the extracts of these leaf samples, DNCC-33, NCC-36 and NCC-44 were identified (see Fig. 5, for chemical formulae and nomenclature). **B.** UV- and mass spectral characterization of PBs from green wild type Arabidopsis leaf samples #6 (UV-spectra pictured are from leaf samples #6, positive-ion mass spectra from LC/ESI-MS-data from leaf samples d0-l).

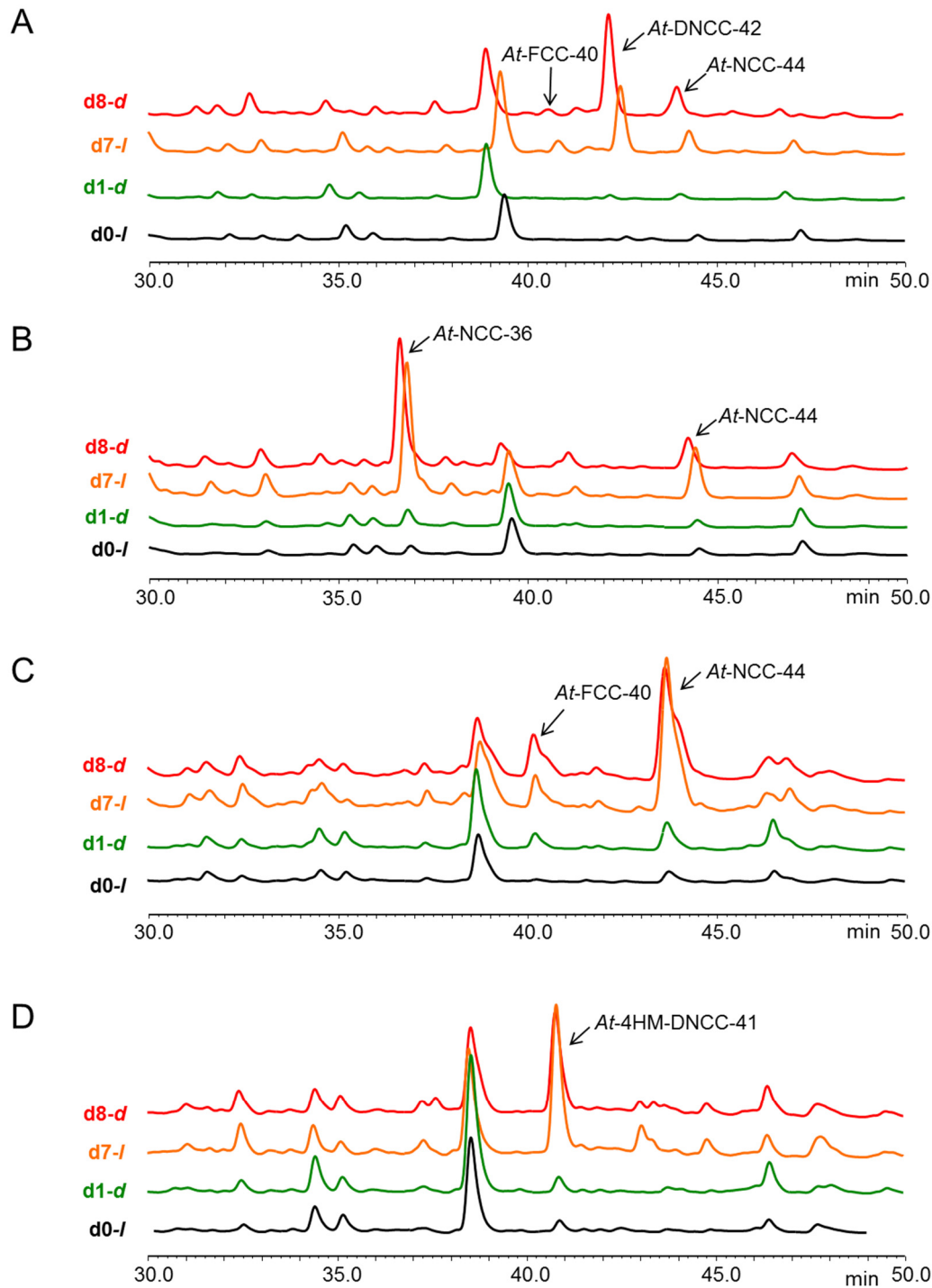


Fig. 4. Phyllobilins in extracts of green leaves of different mutants of *Arabidopsis*. HPLC analysis (detection at 254 nm) of extracts of leaves #6 at sampling times d0-l, d1-d, d7-l and d8-d. **A**, *mes16-1*; **B**, *cyp89a9-1*; **C**, *cyp89a9-1/mes16-1*; **D**, *tic55-3*. See Fig. 5 for chemical formulae of phyllobilins and Supplementary Fig. 3 for corresponding traces of leaf #8 samples.

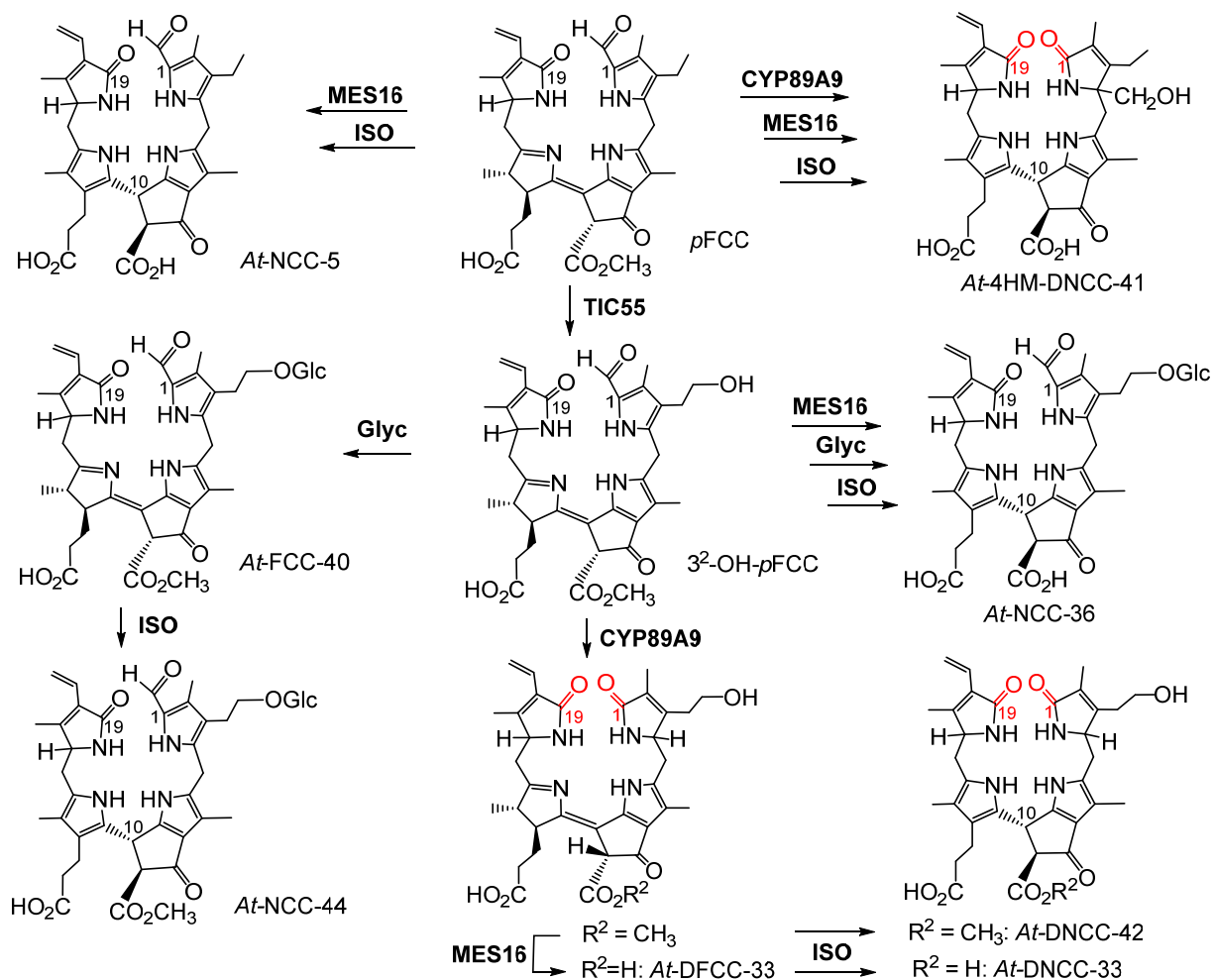


Fig. 5. Colorless phyllobilins detected in leaves of *Arabidopsis* and their proposed formation along the PAO/phyllobilin pathway from *p*FCC. Chemical formulae and abbreviated phenomenological names of the detected seven phyllobilins (PBs) are depicted, as are the enzymes TIC55, CYP89A9, MES16, Glyc (unknown glycosidase) involved in their formation; ISO, non-enzymatic isomerization; 1-oxo and 19-oxo groups of type-II PBs are highlighted red.

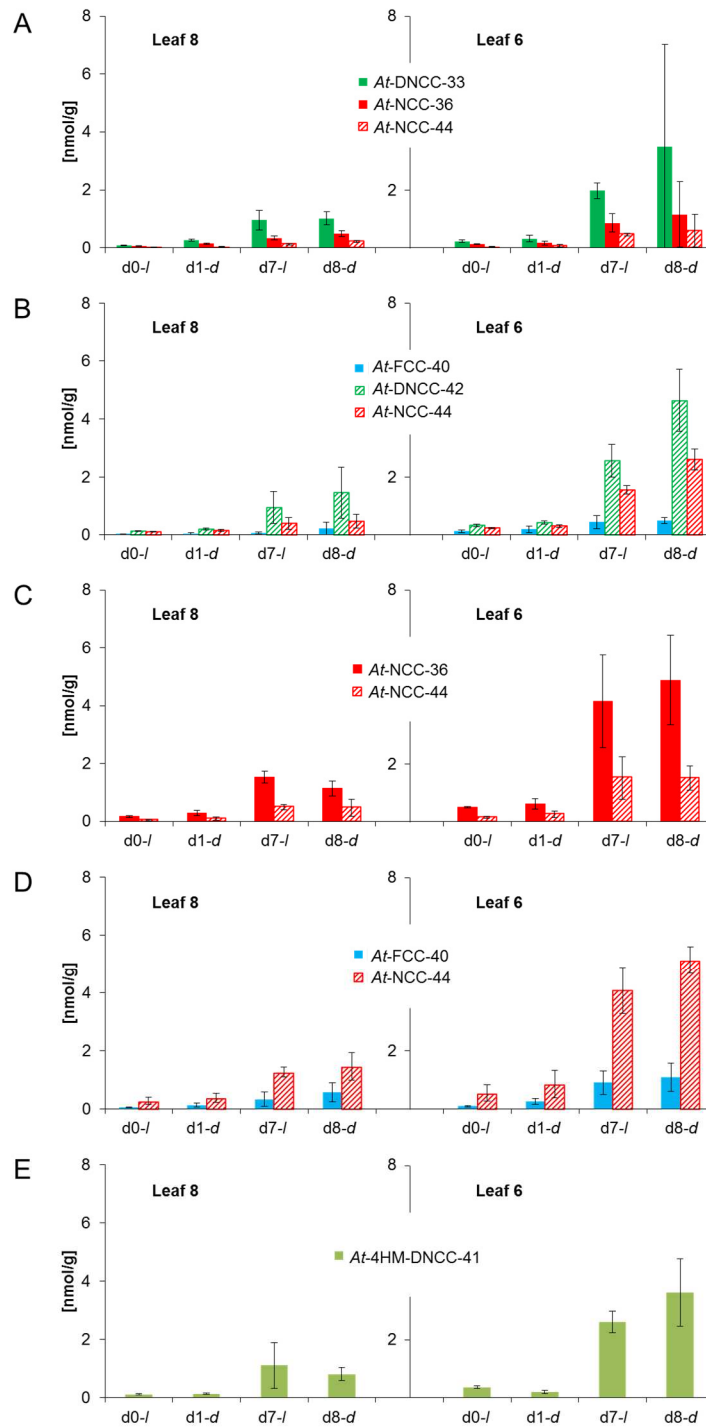


Fig. 6. HPLC-based quantification of phyllobilins detected in green leaves of Arabidopsis. Phyllobilins were analyzed by HPLC in extracts of green leaves #6 and #8 of Arabidopsis at the sampling time points d0-l, d1-d, d7-l and d8-d. **A**, wild type; **B**, *mes16-1*; **C**, *cyp89a9-1*; **D**, *cyp89a9-1/mes16-1*; **E**, *tic55-3*. For identification of phyllobilins in each line, see Figs. 3 and 4; for details of the quantification, see Materials and Methods and Supplementary Material. Data are mean \pm SD of three replicates.

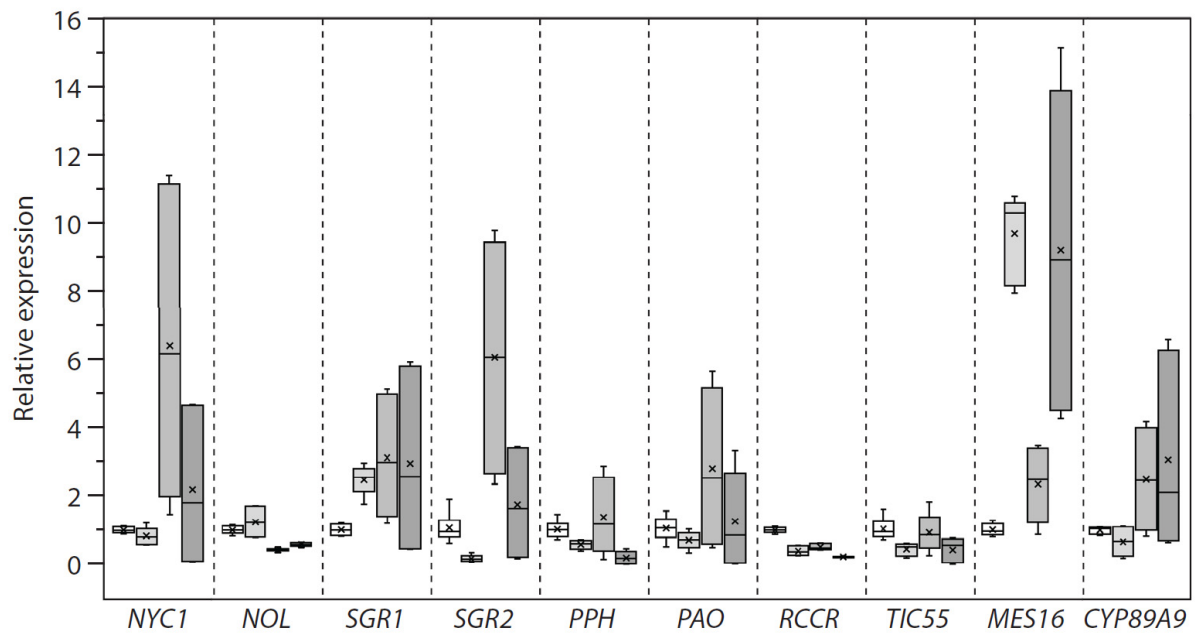


Fig. 7. CCE gene expression in green leaves of Arabidopsis. Box plot of CCE gene expression in wild type Arabidopsis leaf #8 as analyzed by qPCR using *UBQ5* expression for normalization. For each gene, four time points, i.e. d0-l (white), d1-d (light gray), d7-l (middle gray) and d8-d (dark gray) were used and expression was set to 1 for the d0-l sampling point. For gene abbreviations see text.

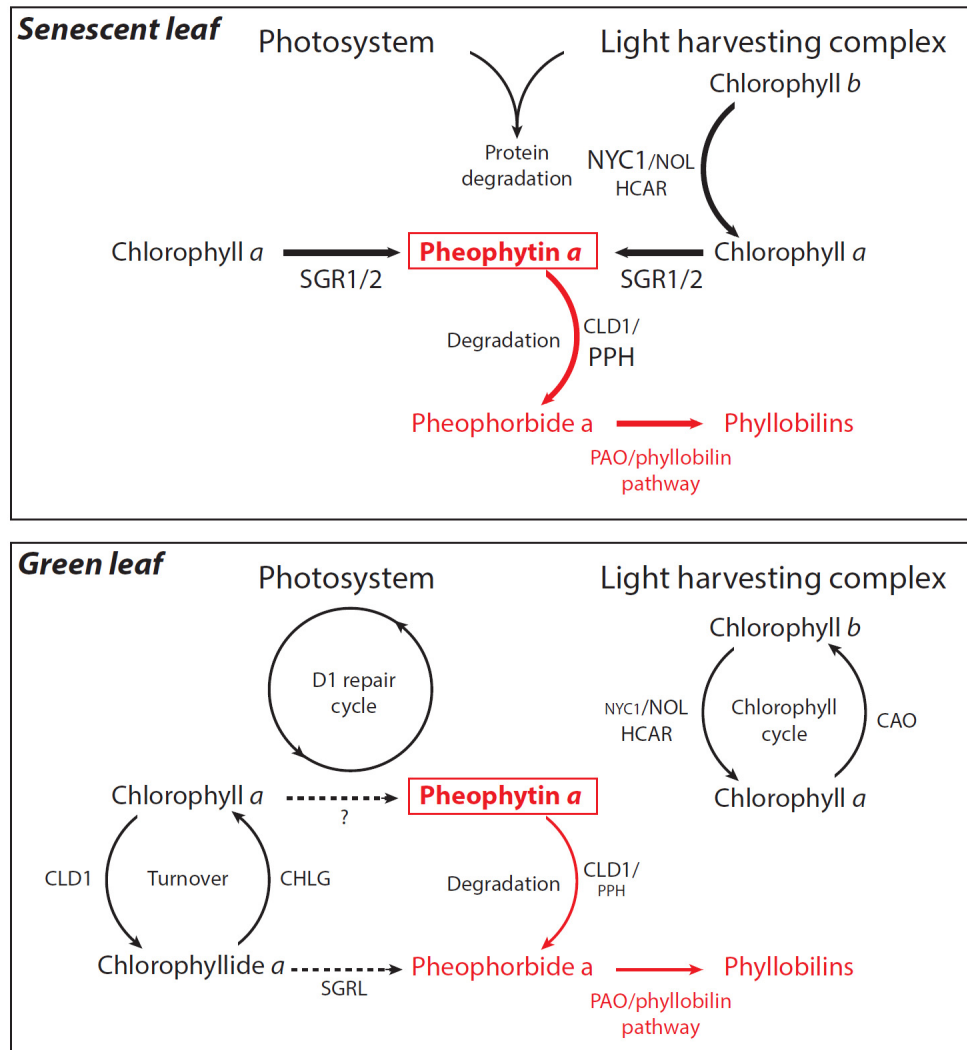


Fig. 8. Models of Chl degradation in senescent and green leaves. In senescent leaves (**top**), Pheide *a* is a key intermediate of the PAO/phyllobilin pathway of massive Chl breakdown, by which Chl *a* and Chl *b* are degraded via Pheide *a*, alongside with the degradation of the protein components of the photosystems. In green leaves (**bottom**), small quantities of phyllobilins are formed from Pheide *a* via the PAO/phyllobilin pathway of Chl breakdown. Pheide *a* may originate mainly from the repair cycle of photosystem II components (D1 protein). Chl *a*, the dominant photoactive cofactor is turned over without net loss, by dephytylation to Chlide *a* by CLD1, and rephytylation to Chl *a* by CHLG. However, Pheide *a* is converted to Pheophorbide *a*, which cannot be reconverted to Pheide *a*, but is degraded by the PAO/phyllobilin pathway. Key players of these processes are depicted; relative fluxes are indicated by arrow thickness. For abbreviations of genes and enzymes, see text.